Electromagnetically induced transparency and Autler-Townes splitting in superconducting flux quantum circuits

Hui-Chen Sun,[1,2] Yu-xi Liu,[1,2,3,*] Hou Ian,[4] J. Q. You,[2,5] E. Il'ichev,[6,7] and Franco Nori[2,8]
[1]*Institute of Microelectronics, Tsinghua University, Beijing 100084, China*
[2]*CEMS, RIKEN, Saitama 351-0198, Japan*
[3]*Tsinghua National Laboratory for Information Science and Technology (TNList), Beijing 100084, China*
[4]*Institute of Applied Physics and Materials Engineering, FST, University of Macau, Macau*
[5]*Beijing Computational Science Research Center, Beijing 100084, China*
[6]*Leibniz Institute of Photonic Technology, D-07702 Jena, Germany*
[7]*Novosibirsk State Technical University, 20 Karl Marx Avenue, 630092 Novosibirsk, Russia*
[8]*Physics Department, The University of Michigan, Ann Arbor, Michigan 48109-1040, USA*
(Received 4 December 2013; revised manuscript received 4 May 2014; published 26 June 2014)

We study the microwave absorption of a driven three-level quantum system, which is realized by a superconducting flux quantum circuit (SFQC), with a magnetic driving field applied to the two upper levels. The interaction between the three-level system and its environment is studied within the Born-Markov approximation, and we take into account the effects of the driving field on the damping rates of the three-level system. We study the linear response of the driven three-level SFQC to a weak probe field. The linear magnetic susceptibility of the SFQC can be changed by both the driving field and the bias magnetic flux. When the bias magnetic flux is at the optimal point, the transition from the ground state to the second-excited state is forbidden and the three-level SFQC has a ladder-type transition. Thus, the SFQC responds to the probe field like natural atoms with ladder-type transitions. However, when the bias magnetic flux deviates from the optimal point, the three-level SFQC has a cyclic transition, thus it responds to the probe field like a combination of natural atoms with ladder-type transitions and natural atoms with Λ-type transitions. In particular, we provide detailed discussions on the conditions for realizing electromagnetically induced transparency and Autler-Townes splitting in three-level SFQCs.

DOI: 10.1103/PhysRevA.89.063822 PACS number(s): 42.50.Gy, 42.50.Ct, 74.50.+r, 85.25.Cp

I. INTRODUCTION

Superconducting quantum circuits (SQCs) with Josephson junctions have been experimentally demonstrated to possess quantized energy levels (e.g., see reviews [1–7]), which are analogous to the quantized internal levels of natural atoms. However, in contrast to natural atoms, the quantized energy levels of SQCs can be tuned by externally controllable parameters. These artificially fabricated SQCs have been extensively explored as qubits in quantum information processing. They also provide us a controllable platform to test fundamental quantum phenomena at a macroscopic scale. For example, quantum interference via Landau-Zener-Stückelberg transitions [8–10] has been experimentally demonstrated in SQCs [11–16]. Moreover, circuit quantum electrodynamics (circuit QED) of SQCs has been extensively explored (e.g., see Refs. [17–21]). Furthermore, the Sisyphus cooling of a harmonic oscillator via a superconducting flux quantum circuit (SFQC) [22] has also been studied [23–26] theoretically and experimentally. Our theoretical prediction on the coexistence of one- and two-photon transitions [27] in three-level SFQCs has been experimentally demonstrated [28]. This coexistence results from the controllable symmetry of the Hamiltonian for SFQCs [27], which are very different from natural atoms.

For three-level SQCs, quantum state control has been theoretically studied in Λ-type transition configurations (e.g., Refs. [29–32]). The microwave-induced cooling of a superconducting qubit via the third energy level has been experimentally demonstrated [33]. This mechanism can be further used to cool the environment surrounding the qubit [34]. The inverse process of cooling [33] can be used for single-photon production [35] and lasing [26], which has been experimentally demonstrated using superconducting charge quantum circuits [36]. SQCs also allow us to experimentally explore atomic-physics phenomena [5,6] on microelectronic chips, e.g., electromagnetically induced transparency (EIT) [37,39–41] and Autler-Townes splitting (ATS) [42]. EIT and ATS both display a dip in the absorption spectrum of a three-level quantum system to a weak resonant probe field when a strong driving field is appropriately applied. However, EIT is due to Fano interference [43], while ATS is due to the driving-field-induced shift of the transition frequency which is probed. The application of EIT in atomic systems to nonlinear optics [41] and quantum information theory [44] has been extensively studied.

In this paper, we study the linear response of a three-level SFQC to a weak probe field when the two upper levels are driven by a strong external microwave field. Our motivation is given as follows:

(1) The microwave-induced transitions between different energy levels of SFQCs can be adjusted by the bias magnetic flux [27]; thus, the linear response of SFQCs should depend on the magnetic bias.

(2) EIT has been proposed as a promising method to probe the coherence of superconducting qubit states [45,46]. Tunable EIT has been studied in circuit QED systems by using dressed states [47]. Moreover, ATS [48–53] and coherent population trapping [54] have been experimentally demonstrated in different types of SQCs with three energy levels. ATS has

*yuxiliu@mail.tsinghua.edu.cn

been proposed as a basis for fast, high on-off ratio microwave routers [49,52].

(3) A theoretical study [51] proposed an objective test of experimental data based on the Akaike information criterion for discerning EIT from ATS. This objective test was then applied in an experiment [55] in natural atomic systems and an experiment [56] in whispering-gallery-mode optical resonators. Both experiments [55,56] demonstrated the transition from EIT to ATS.

(4) One experiment [50] in three-level SFQCs showed that the two peaks in the transmission spectrum for ATS [51] have different heights, even when the driving field is resonantly applied.

(5) Using weak continuous measurements [57–62], experimentalists studied magnetic susceptibilities to extract the information of SQCs [63–66].

This study mainly focuses on the following questions: (i) how the linear response of SFQCs changes with the tunable bias magnetic flux; (ii) what are the differences between the linear responses of SFQCs and natural atoms; (iii) what are the conditions for realizing EIT and ATS in three-level SFQCs; (iv) why the transmission spectrum in the ATS experiment [50,51] is asymmetric.

Differences between our study for EIT with those in Refs. [45,46] are as follows: (i) We consider the effect of the driving field on the dissipation of SFQCs by using the method developed in Refs. [67–70]. (ii) References [45,46] study EIT in the basis of the single-well states of SFQCs, which have a Λ-type transition. However, our study is in the basis of the three lowest eigenstates of SFQCs, which have a ladder-type transition (or cyclic transition) when the bias magnetic flux is at (or deviates from) the optimal point [27]. (iii) Moreover, we provide detailed discussions on the relation between EIT and ATS for SFQCs.

Our paper is organized as follows. In Sec. II, we first briefly review the SFQC and write the Hamiltonian of the three-level SFQC, which interacts with the strong driving field, the weak probe field, and the environment. We also give the definition of the linear magnetic susceptibility of the three-level SFQC to a weak probe magnetic field. In Sec. III, formal solutions of the operators of the three-level SFQC are given by solving the Heisenberg-Langevin equations. In Sec. IV, magnetic susceptibilities of the three-level SFQC are calculated and the conditions for realizing EIT and ATS are derived. We finally give conclusions in Sec. V.

II. THEORETICAL MODEL

A. Hamiltonian of superconducting flux qubit circuits

We study a SFQC, as shown in Fig. 1(a), consisting of three Josephson junctions in a superconducting loop with negligible self-inductance. Two junctions have equal size, each with Josephson energy E_J and capacitance C_J. The third one, which is smaller than the others, has a Josephson energy αE_J and capacitance αC_J, with $0.5 < \alpha < 1$. The SFQC is threaded by a bias magnetic flux (dc) Φ_e and driven by a strong time-dependent magnetic flux (ac) $\Phi_D(t)$. A weak magnetic flux $\Phi_P(t)$ as a probe field is also applied to the SFQC. If the driving $\Phi_D(t)$ and the probe $\Phi_P(t)$ fields are not applied, then

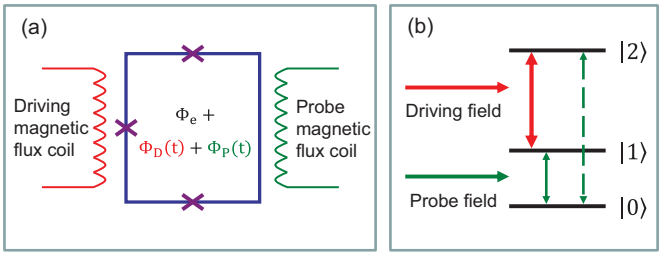

FIG. 1. (Color online) (a) Schematic diagram of a SFQC with three Josephson junctions. Here, Φ_e is a bias magnetic flux (dc), while $\Phi_D(t) = \Phi_c \cos(\omega_0 t)$ is a strong driving magnetic flux (ac) provided by the left coil (in red color), $\Phi_P(t)$ is a weak probe magnetic flux (ac) provided by the right coil (in green color). (b) Schematic diagram of the three-level SFQC. The driving field is used to couple the two upper energy levels $|1\rangle$ and $|2\rangle$. However, the probe field is used to couple the energy levels $|0\rangle$ and $|1\rangle$, as well as the energy levels $|0\rangle$ and $|2\rangle$.

the Hamiltonian of the SFQC with a dc bias Φ_e is written as (e.g., in Refs. [22,27])

$$H_0 = \frac{P_p^2}{2M_p} + \frac{P_m^2}{2M_m} + U(\varphi_p,\varphi_m), \tag{1}$$

with effective masses $M_p = 2C_J(\Phi_0/2\pi)^2$ and $M_m = M_p(1 + 2\alpha)$. Here, Φ_0 is the flux quantum. The quantum conjugate variables φ_p and φ_m of the effective momenta P_p and P_m, respectively, are defined by $\varphi_p = (\varphi_1 + \varphi_2)/2$ and $\varphi_m = (\varphi_2 - \varphi_1)/2$, with the phase drops φ_1 and φ_2 across the two larger junctions. The potential energy $U(\varphi_p,\varphi_m)$ is

$$U(\varphi_p,\varphi_m) = 2E_J(1 - \cos\varphi_p \cos\varphi_m) + \alpha E_J\,[1 - \cos(2\pi f + 2\varphi_m)]\,, \tag{2}$$

with the reduced magnetic flux $f = \Phi_e/\Phi_0$. The bias magnetic flux Φ_e can be used to adjust the shape of the potential energy between the symmetric double well and the asymmetric double well. Thus, as shown in Fig. 2(a), the eigenvalues E_l of the SFQC can be adjusted by Φ_e (or the reduced magnetic flux f). In the basis of the eigenstates $|l\rangle$, corresponding to the lth eigenvalue E_l, of the Hamiltonian H_0 in Eq. (1), we can rewrite Eq. (1) as

$$H_0 = \sum_{l=0}^{N} E_l\,\sigma_{ll}, \tag{3}$$

with $\sigma_{ll} = |l\rangle\langle l|$. As an example and for concreteness, the eigenvalues E_l of the Hamiltonian in Eq. (1) for the six lowest-energy levels are plotted in Fig. 2(a) as functions of the reduced magnetic flux f with $\alpha = 0.7$ and $E_J/E_c = 48$. Here, the charging energy $E_c = e^2/2C_J$.

B. Hamiltonian of a driven and probed three-level system with its environment

Let us now only consider the three lowest-energy levels of the SFQC as in Refs. [27,34,35]. That is, the free Hamiltonian of the SFQC can be given by Eq. (3) with $l = 0, 1, 2$. As schematically shown in Fig. 1(b), when the driving $\Phi_D(t)$ and the probe $\Phi_P(t)$ fields are applied to the three-level SFQC, the

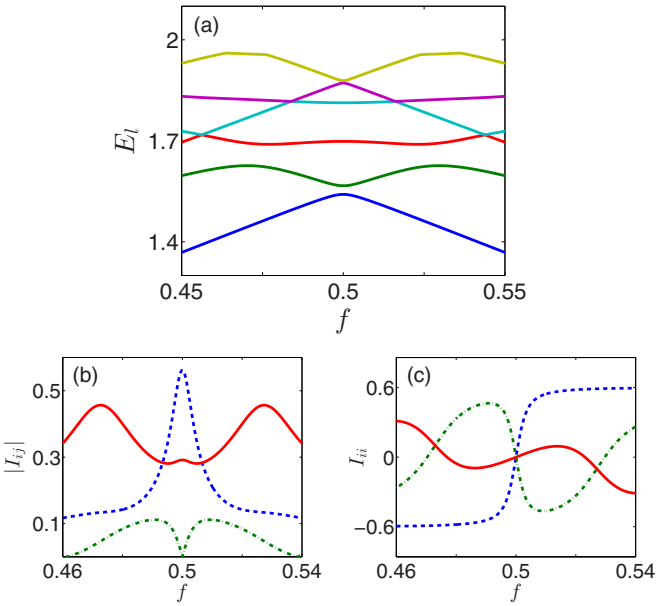

FIG. 2. (Color online) (a) Eigenvalues E_l of the SFQC versus the reduced magnetic flux f, in units of E_J, for the six lowest-energy levels. (b) Moduli of the loop current transition matrix elements $|I_{ij}|$ $(i < j)$ for the three lowest-energy levels ($|0\rangle$, $|1\rangle$, and $|2\rangle$) versus the reduced magnetic flux f for $|I_{01}|$ (blue dashed curve), $|I_{02}|$ (green dashed-dotted curve), and $|I_{12}|$ (red solid curve). (c) Loop current diagonal matrix elements I_{ii} for the three lowest-energy levels ($|0\rangle$, $|1\rangle$, and $|2\rangle$) versus the reduced magnetic flux f for I_{00} (blue dashed curve), I_{11} (green dashed-dotted curve), and I_{22} (red solid curve). In (b) and (c), the loop current matrix elements are in units of I_0. Here, we choose $\alpha = 0.7$ and $E_J/E_c = 48$.

Hamiltonian of the three-level SFQC with its environment can be given by

$$H_q = \sum_{l=0}^{2} E_l \sigma_{ll} + \hbar \sum_n \omega_n' b_n^\dagger b_n + H_I. \tag{4}$$

The interaction Hamiltonian H_I is generally given by

$$\begin{aligned} H_I &= H_{I,D} + H_{I,P} + H_{I,E} \\ &= -\Phi_D(t)\hat{I} - \Phi_P(t)\hat{I} - \hbar Q \hat{I}, \end{aligned} \tag{5}$$

where $\hbar Q$ represents the magnetic flux induced by the environment. The operator $\hat{I}$ in Eq. (5) represents the current through the SFQC loop, which can be given as

$$\hat{I} = \sum_{i,j=0}^{2} I_{ij} \sigma_{ij}, \tag{6}$$

with $\sigma_{ij} = |i\rangle\langle j|$ in the basis of the three lowest eigenstates ($|0\rangle$, $|1\rangle$, and $|2\rangle$) of the Hamiltonian in Eq. (1). Here, the matrix elements of the loop current operator $\hat{I}$ are given as $I_{ij} = \langle i|\hat{I}_g|j\rangle$, for the general definition [71] of the loop current operator

$$\hat{I}_g = \frac{\alpha I_0}{1+2\alpha}[2\cos\varphi_p \sin\varphi_m - \sin(2\pi f + 2\varphi_m)], \tag{7}$$

with $I_0 = 2\pi E_J/\Phi_0$. For the completeness of the paper and further numerical discussions, the moduli of the loop current transition matrix elements $|I_{ij}|$ $(i < j)$ in Fig. 2(b) and the loop current diagonal matrix elements I_{ii} in Fig. 2(c) are plotted as functions of the reduced magnetic flux f for the three lowest-energy levels, with the same parameters as in Fig. 2(a). It is clear that these matrix elements can be controlled by the bias magnetic flux Φ_e (or saying f).

The environment is described by multimode harmonic oscillators, each with the creation (annihilation) operator $b_n^\dagger$ (b_n) and frequency ω_n'. The environmental variable is

$$Q = \sum_n \kappa_n (b_n^\dagger + b_n), \tag{8}$$

where κ_n characterizes the coupling between each mode of the environment and the three-level SFQC.

The driving field $\Phi_D(t)$ is assumed to have frequency ω_0 and amplitude Φ_c, resonantly or near resonantly applied to the two upper-energy levels $|1\rangle$ and $|2\rangle$. Thus, in the rotating-wave approximation (RWA), the driving-field-induced Hamiltonian $H_{I,D}$ in Eq. (5) can be given as

$$H_{I,D} = \hbar\Omega_D \exp(i\omega_0 t)\sigma_{12} + \hbar\Omega_D^* \exp(-i\omega_0 t)\sigma_{21}. \tag{9}$$

The coupling constant Ω_D between the driving field $\Phi_D(t)$ and the three-level SFQC is

$$\Omega_D = -\frac{1}{2\hbar}\Phi_c I_{12}, \tag{10}$$

with I_{12} given in Eq. (6) for $i = 1$ and $j = 2$. The Rabi frequency of the driving field is given by the modulus $|\Omega_D|$ of the coupling constant.

In contrast to the driving field $\Phi_D(t)$, in this study, we assumed that the probe field $\Phi_P(t)$ includes two components which can induce either the $|0\rangle \leftrightarrow |1\rangle$ transition or the $|0\rangle \leftrightarrow |2\rangle$ transition. Thus, under the RWA, the probe-field-induced Hamiltonian $H_{I,P}$ in Eq. (5) can be given as

$$H_{I,P} = -\Phi_P(t)\left(\sum_{i=1}^{2} I_{0i}\sigma_{0i} + \text{H.c.}\right). \tag{11}$$

Based on the above discussions, the total Hamiltonian of the driven and probed three-level SFQC with its environment can be given by

$$\begin{aligned} H = &\sum_{l=0}^{2} E_l \sigma_{ll} + \hbar \sum_n \omega_n' b_n^\dagger b_n \\ &+ \hbar\Omega_D \exp(i\omega_0 t)\sigma_{12} + \hbar\Omega_D^* \exp(-i\omega_0 t)\sigma_{21} \\ &- \Phi_P(t)\left(\sum_{i=1}^{2} I_{0i}\sigma_{0i} + \text{H.c.}\right) - \hbar Q\hat{I}, \end{aligned} \tag{12}$$

with $\hat{I}$ given in Eq. (6).

We emphasize that the Hamiltonian of the SFQC in Eq. (1) has a well-defined parity when the bias magnetic flux is at the optimal point, i.e., $f = 0.5$. In this case, the transition between the energy levels $|0\rangle$ and $|2\rangle$ is forbidden and the selection rule in SFQCs is the same as in natural atoms [27], thus, the three-level SFQC has a ladder-type transition, and the probe field can only couple the energy levels $|0\rangle$ and $|1\rangle$. However, when the bias magnetic flux deviates from the optimal point, i.e., $f \neq 0.5$, the parity of the Hamiltonian in Eq. (1) related to

the variables φ_p and φ_m is broken and any transition between two of the three lowest-energy levels is possible. In this case, the three-level SFQC has a cyclic transition [27] and the probe field can couple the energy levels $|0\rangle$ and $|1\rangle$, as well as the energy levels $|0\rangle$ and $|2\rangle$. This is a very important difference between three-level SFQCs and three-level natural atoms.

C. Magnetic susceptibility of three-level SFQCs

The linear response of the three-level SFQC to the probe field can be characterized by the linear magnetic susceptibility. By taking the same arguments and calculation method as in Ref. [70], the linear magnetic susceptibility $\chi_q(\omega)$ of the three-level SFQC to the probe field $\Phi_{\rm P}(t)$ can be obtained via the following Fourier transform:

$$\left\langle \frac{\delta \hat{I}(t)}{\delta \Phi_{\rm P}(t_1)} \right\rangle = \int \frac{d\omega}{2\pi} \chi_q(\omega) \exp[-i\omega(t-t_1)]. \tag{13}$$

Note that in this paper we use the integral sign $\int$ to denote the integration over the whole real axes, i.e., $\int \equiv \int_{-\infty}^{\infty}$. The real and imaginary parts of the magnetic susceptibility $\chi_q(\omega)$ are used to characterize, respectively, the dispersion and the absorption of the probe field by the three-level SFQC. The parameter $\hat{I}(t)$ in Eq. (13) is the loop current operator in the Heisenberg picture and is given via Eq. (6) as

$$\hat{I}(t) = \sum_{i,j=0}^{2} I_{ij}\, \sigma_{ij}(t). \tag{14}$$

Here, $\sigma_{ij}(t)$ denotes the operator σ_{ij} in the Heisenberg picture. Note that the difference of the susceptibility between the three-level SFQCs in Eq. (13) and the superconducting qubits in Ref. [70] only involves replacing the loop current operator of the superconducting qubits by that of the three-level SFQCs. However, this simple replacement will result in many new results, as discussed below.

III. EQUATIONS OF MOTION AND SOLUTIONS OF OPERATORS

A. Heisenberg equations and correlation functions

To obtain the magnetic susceptibility $\chi_q(\omega)$ of the three-level SFQC, we need to obtain the expression of the loop current operator $\hat{I}(t)$, which can be expressed in terms of operators $\sigma_{lm}(t)$. Thus, we first solve the equations of motion for all operators $\sigma_{lm}(t)$. In the rotating reference frame with the unitary transform

$$U(t) = \exp(-i\omega_1\sigma_{11}\, t - i\omega'\sigma_{22}\, t), \tag{15}$$

the Hamiltonian in Eq. (12) can be transformed as

$$H_r = \hbar\Delta\sigma_{22} + \hbar\Omega_{\rm D}\sigma_{12} + \hbar\Omega_{\rm D}^{*}\sigma_{21} + \hbar\sum_n \omega_n' b_n^{\dagger} b_n - \Phi_{\rm P}(t)(I_{01}\sigma_{01}e^{-i\omega_1 t} + I_{02}\sigma_{02}e^{-i\omega' t} + {\rm H.c.}) - \hbar Q\hat{I}_r, \tag{16}$$

with the loop current operator $\hat{I}$ in the rotating reference frame

$$\hat{I}_r = [I_{01}\sigma_{01}e^{-i\omega_1 t} + I_{02}\sigma_{02}e^{-i\omega' t} + I_{12}\sigma_{12}e^{-i\omega_0 t} + {\rm H.c.}] + \sum_{i=0}^{2} I_{ii}\sigma_{ii}. \tag{17}$$

Here, we define the transition frequencies ω_i $(i = 1, 2, 3)$ of the three-level SFQC as $\omega_1 = (E_1 - E_0)/\hbar$, $\omega_2 = (E_2 - E_0)/\hbar$, and $\omega_3 = (E_2 - E_1)/\hbar$. The parameter $\Delta = \omega_3 - \omega_0$ is the detuning between the frequency ω_0 of the driving field and the transition frequency ω_3. And, $\omega' = \omega_0 + \omega_1 = \omega_2 - \Delta$. In the derivation of Eq. (16), we have used the completeness relation $|0\rangle\langle 0| + |1\rangle\langle 1| + |2\rangle\langle 2| = 1$ for the three-level SFQC and neglected the constant term. With the Hamiltonian H_r in Eq. (16), the Heisenberg equation of motion for any operator $\sigma_{lm}(t)$ in the rotating reference frame can be given by

$$\frac{\partial \sigma_{lm}(t)}{\partial t} = \frac{1}{i\hbar}[\sigma_{lm}(t), H_r]_{-}. \tag{18}$$

The environment has an infinite number of degrees of freedom, thus it is usually considered as a macroscopic system and assumed in a thermodynamic equilibrium state. If the free environmental variable $Q^{(0)}(t)$,

$$Q^{(0)}(t) = \sum_n \kappa_n [b_n^{\dagger}(0)e^{i\omega_n' t} + b_n(0)e^{-i\omega_n' t}], \tag{19}$$

obeys Gaussian fluctuations or the interaction between the three-level SFQC and its environment is weak [67], the environmental operator Q in Eq. (16) has the following solution in the Heisenberg picture:

$$Q(t) = Q^{(0)}(t) + \int_{-\infty}^{t} dt'\, \phi(t,t')\, \hat{I}_r(t'). \tag{20}$$

Note that $b_n^{\dagger}(0)$ and $b_n(0)$ in Eq. (19) are the creation and annihilation operators of the nth environmental bosonic mode at the initial time. The environmental linear response function $\phi(t,t')$ is defined as the correlation function of the free environmental variables averaged over the environmental equilibrium state

$$\phi(t,t') = \langle i[Q^{(0)}(t), Q^{(0)}(t')]_{-}\rangle_{\rm E}\, \theta(t-t'), \tag{21}$$

where the Heaviside step function $\theta(t-t') = 1$ for $t - t' > 0$, but $\theta(t-t') = 0$ for $t - t' < 0$. The environmental susceptibility $\chi(\omega)$ is defined [67] by the Fourier transform of the response function $\phi(t,t')$:

$$\chi(\omega) = \chi'(\omega) + i\chi''(\omega) = \int d\tau\, \phi(\tau)\, \exp(i\omega\tau), \tag{22}$$

with the time interval $\tau = t - t'$ and

$$\chi'(\omega) = -\frac{1}{\pi}\, \wp \int d\omega'\, \frac{\chi''(\omega')}{\omega - \omega'}. \tag{23}$$

Here, $\wp$ stands for the Cauchy principal value.

Using the method developed in Refs. [67–70], the product operators $\sigma_{lm}(t)Q(t)$ can be written as

$$\sigma_{lm}(t)Q(t) = \frac{1}{2}\int dt'\phi(t,t')[\sigma_{lm}(t), \hat{I}_r(t')]_{+} + \xi_{lm}(t) + i\int dt'\widetilde{M}(t,t')[\sigma_{lm}(t), \hat{I}_r(t')]_{-}. \tag{24}$$

Here, the upper bound of the integral in Eq. (24) has been extended from the time t to ∞ by using the step function $\theta(t-t') = 0$ for $t' > t$. The fluctuation force $\xi_{lm}(t)$ in Eq. (24), which has zero average value over the environmental

equilibrium state, is expressed as

$$\xi_{lm}(t) = \frac{1}{2}[\sigma_{lm}(t), Q^{(0)}(t)]_+ - i\int dt' \widetilde{M}(t,t')[\sigma_{lm}(t), \hat{I}_r(t')]_-, \quad (25)$$

with the causal correlation function $\widetilde{M}(t,t') = M(t,t')\theta(t-t')$. The symmetrized correlation function $M(t,t')$ of the free environmental variable $Q^{(0)}(t)$ is defined by

$$M(t,t') = \tfrac{1}{2}\langle [Q^{(0)}(t), Q^{(0)}(t')]_+\rangle_{\rm E}, \quad (26)$$

with the average over the environmental equilibrium state. Here, we need to mention that the Born approximation is made when we take the average over the environmental equilibrium state in Eqs. (21) and (26). That is, the states of the three-level SFQC and the environment are factorized at any time and the environment is always assumed in its equilibrium state. The spectral density $S(\omega)$ is defined [67] by the Fourier transform of the correlation function $M(t,t')$:

$$S(\omega) = \int d\tau\, M(\tau)\, \exp(i\omega\tau). \quad (27)$$

The Fourier transform $\widetilde{S}(\omega)$ of the correlation function $\widetilde{M}(\tau)$ can be given as [67]

$$\widetilde{S}(\omega) = \tfrac{1}{2}[S(\omega) + iS'(\omega)], \quad (28)$$

with

$$S'(\omega) = \frac{1}{\pi}\wp\int d\omega' \frac{S(\omega')}{\omega-\omega'}. \quad (29)$$

B. Quantum Langevin equations

Using Eqs. (17) and (24), we can rewrite the Heisenberg equation in Eq. (18) into a quantum Langevin equation. For example, the operator $\sigma_{01}(t)$ obeys the following quantum Langevin equation:

$$\begin{aligned}\frac{\partial\sigma_{01}(t)}{\partial t} &= i\frac{|I_{01}|^2}{2}\int dt'[S^{(+)}_{00,01}(t,t') + iS^{(-)}_{00,01}(t,t')]e^{i\omega_1\tau} \\ &- i\frac{|I_{01}|^2}{2}\int dt'[S^{(+)}_{11,01}(t,t') + iS^{(-)}_{11,01}(t,t')]e^{i\omega_1\tau} \\ &- i\frac{|I_{02}|^2}{2}\int dt'[S^{(+)}_{21,02}(t,t') + iS^{(-)}_{21,02}(t,t')]e^{i\omega'\tau} \\ &+ i\frac{|I_{12}|^2}{2}\int dt'[S^{(+)}_{02,21}(t,t') + iS^{(-)}_{02,21}(t,t')]e^{-i\omega_0\tau} \\ &- i\frac{(I_{00}-I_{11})I_{00}}{2}\int dt'[S^{(+)}_{01,00}(t,t') + iS^{(-)}_{01,00}(t,t')] \\ &- i\frac{(I_{00}-I_{11})I_{11}}{2}\int dt'[S^{(+)}_{01,11}(t,t') + iS^{(-)}_{01,11}(t,t')] \\ &- i\frac{(I_{00}-I_{11})I_{22}}{2}\int dt'[S^{(+)}_{01,22}(t,t') + iS^{(-)}_{01,22}(t,t')] \\ &- i\Omega_{\rm D}\sigma_{02}(t) + \frac{i}{\hbar}\Phi_{\rm P}(t)I_{10}[\sigma_{00}(t)-\sigma_{11}(t)]e^{i\omega_1 t} \\ &- \frac{i}{\hbar}\Phi_{\rm P}(t)I_{20}\sigma_{21}(t)e^{i\omega' t} + iI_{10}[\xi_{00}(t)-\xi_{11}(t)]e^{i\omega_1 t} \\ &- iI_{20}\xi_{21}(t)e^{i\omega' t} + iI_{12}\xi_{02}(t)e^{-i\omega_0 t} \\ &- i(I_{00}-I_{11})\xi_{01}(t). \end{aligned} \quad (30)$$

The commutators $S^{(+)}_{ij,lm}(t,t')$ and anticommutators $S^{(-)}_{ij,lm}(t,t')$ in Eq. (30) are defined as

$$S^{(+)}_{ij,lm}(t,t') = \varphi(t,t')[\sigma_{ij}(t), \sigma_{lm}(t')]_+, \quad (31)$$

$$S^{(-)}_{ij,lm}(t,t') = 2\widetilde{M}(t,t')[\sigma_{ij}(t), \sigma_{lm}(t')]_-. \quad (32)$$

The fluctuation forces $\xi_{lm}(t)$ in Eq. (30) can be given by Eq. (25). However, we are only interested in the average dynamics of the three-level SFQC operators in our following discussions and not interested in the correlation of the fluctuation forces; thus, hereafter we average Eq. (30) over the environmental equilibrium state, and the fluctuation forces $\xi_{lm}(t)$ become zero. Under the integral in Eq. (30), we only keep the terms with exponential factors including the time interval τ, e.g., $\exp(-i\omega_0\tau)$, and the terms without exponential factors. Other fast-oscillating terms with exponential factors, e.g., $\exp(i\omega_1 t - i\omega_0 t')$, have been neglected under the integral in Eq. (30) because the contributions of these terms are negligibly small.

To obtain each integral in Eq. (30), we have to first calculate the commutators $S^{(+)}_{ij,lm}(t,t')$ and anticommutators $S^{(-)}_{ij,lm}(t,t')$ with expressions $[\sigma_{ij}(t),\sigma_{lm}(t')]_\pm$ in Eqs. (31) and (32). With the assumptions that the coupling between the three-level SFQC and its environment is weak, and that the environmental correlation time τ_c is very small, the relaxation of the three-level SFQC is negligible during the environmental correlation time τ_c. Thus, the Bloch-Redfield approximation can be applied and the operators $\sigma_{lm}(t')$ in Eqs. (31) and (32) can be approximately obtained by neglecting the interaction between the three-level SFQC and its environment. In this case, the operators $\sigma_{lm}(t')$ can be easily expressed in terms of the operators at the moment t and the time interval τ. For example, the operator $\sigma_{01}(t')$ can be expressed as

$$\sigma_{01}(t') = e^{i\frac{\Delta}{2}\tau}A^*(\tau)\sigma_{01}(t) + ie^{i\frac{\Delta}{2}\tau}B(\tau)\sigma_{02}(t). \quad (33)$$

Here,

$$A(\tau) = \cos\left(\frac{\Omega\tau}{2}\right) + i\sin\left(\frac{\Omega\tau}{2}\right)\cos 2\theta, \quad (34)$$

$$B(\tau) = \nu\sin\left(\frac{\Omega\tau}{2}\right)\sin 2\theta, \quad (35)$$

with $\Omega = \sqrt{\Delta^2 + 4|\Omega_{\rm D}|^2}$ and $\nu = \Omega_{\rm D}/|\Omega_{\rm D}|$. The detailed calculations on the operators $\sigma_{lm}(t')$ are given in Appendix A. Using the relation of simultaneous operators $\sigma_{ij}(t)\sigma_{lm}(t) = \sigma_{im}(t)\delta_{jl}$, the commutators and anticommutators in Eqs. (31) and (32) can be expressed by the operators at the moment t and the time interval τ. Thus, substituting the operator relations (see Appendix A) as in Eq. (33) into Eq. (30), and integrating over the time interval τ, the quantum Langevin equation (30) can be simplified.

Based on the discussions above, the quantum Langevin equations of other operators can also be derived by using the same approach as for Eq. (30). All of the quantum Langevin equations related to the operators $\sigma_{lm}(t)$ after averaging over

the environmental equilibrium state are given as follows:

$$\frac{\partial\sigma_{01}(t)}{\partial t} = i\Gamma_{11}\sigma_{01}(t) + i(\Gamma_{12}-\Omega_{\rm D})\sigma_{02}(t) + \frac{i}{\hbar}\Phi_{\rm P}(t)I_{10}[\sigma_{00}(t)-\sigma_{11}(t)]e^{i\omega_1 t} - \frac{i}{\hbar}\Phi_{\rm P}(t)I_{20}\sigma_{21}(t)e^{i\omega' t}, \quad (36)$$

$$\frac{\partial\sigma_{02}(t)}{\partial t} = i(\Gamma_{21}-\Omega_{\rm D}^{*})\sigma_{01}(t) + i(\Gamma_{22}-\Delta)\sigma_{02}(t) + \frac{i}{\hbar}\Phi_{\rm P}(t)I_{20}[\sigma_{00}(t)-\sigma_{22}(t)]e^{i\omega' t} - \frac{i}{\hbar}\Phi_{\rm P}(t)I_{10}\sigma_{12}(t)e^{i\omega_1 t}, \quad (37)$$

$$\frac{\partial\sigma_{12}(t)}{\partial t} = i(\Gamma_{31}-\Delta)\sigma_{12}(t) + i\Gamma_{32}\sigma_{21}(t) + i\Gamma_{33}\sigma_{00}(t) + i(\Gamma_{34}-\Omega_{\rm D}^{*})\sigma_{11}(t) + i(\Gamma_{35}+\Omega_{\rm D}^{*})\sigma_{22}(t) + \frac{i}{\hbar}\Phi_{\rm P}(t)[I_{20}\sigma_{10}(t)e^{i\omega' t} - I_{01}\sigma_{02}(t)e^{-i\omega_1 t}], \quad (38)$$

$$\frac{\partial\sigma_{00}(t)}{\partial t} = i\Gamma_{41}\sigma_{00}(t) + i\Gamma_{42}\sigma_{11}(t) + i\Gamma_{43}\sigma_{22}(t) + i\Gamma_{44}\sigma_{12}(t) + i\Gamma_{45}\sigma_{21}(t) + \frac{\Phi_{\rm P}(t)}{\hbar}[iI_{01}\sigma_{01}(t)e^{-i\omega_1 t} + iI_{02}\sigma_{02}(t)e^{-i\omega' t} + \text{H.c.}], \quad (39)$$

$$\frac{\partial\sigma_{11}(t)}{\partial t} = i\Gamma_{51}\sigma_{00}(t) + i\Gamma_{52}\sigma_{11}(t) + i\Gamma_{53}\sigma_{22}(t) + i(\Gamma_{54}-\Omega_{\rm D})\sigma_{12}(t) + i(\Gamma_{55}+\Omega_{\rm D}^{*})\sigma_{21}(t) + \frac{\Phi_{\rm P}(t)}{\hbar}[iI_{10}\sigma_{10}(t)e^{i\omega_1 t} + iI_{12}\sigma_{12}(t)e^{-i\omega_0 t} + \text{H.c.}], \quad (40)$$

$$\frac{\partial\sigma_{22}(t)}{\partial t} = i\Gamma_{61}\sigma_{00}(t) + i\Gamma_{62}\sigma_{11}(t) + i\Gamma_{63}\sigma_{22}(t) + i(\Gamma_{64}+\Omega_{\rm D})\sigma_{12}(t) + i(\Gamma_{65}-\Omega_{\rm D}^{*})\sigma_{21}(t) + \frac{\Phi_{\rm P}(t)}{\hbar}[iI_{20}\sigma_{20}(t)e^{i\omega' t} + iI_{21}\sigma_{21}(t)e^{i\omega_0 t} + \text{H.c.}]. \quad (41)$$

The expressions for the complex coefficients Γ_{lm} $(l,m=1,2)$ in Eqs. (36) and (37) are given in Appendix B. The expressions for the complex coefficients Γ_{lm} in Eqs. (38)–(41) are not given because they are not used in the following calculations.

C. Steady-state values

We are interested in the linear magnetic susceptibility of the driven three-level SFQC in the steady state; therefore, we need to obtain the steady-state values and the probe-field-dependent average values of the operators σ_{lm} of the three-level SFQC. By averaging Eqs. (36)–(41) over the state of the three-level SFQC in the Heisenberg picture, we can obtain the dynamical equations for the average values $\langle\sigma_{lm}\rangle$. However, we are only interested in the response of the steady state of the three-level SFQC to the probe field, thus, our following calculations are independent of the explicit form of the state of the three-level SFQC in the Heisenberg picture. The steady-state values $\langle\sigma_{lm}^{(s)}\rangle$ can be obtained via the equations for the average values $\langle\sigma_{lm}\rangle$ by setting $\partial\langle\sigma_{lm}(t)\rangle/\partial t = 0$ and $\Phi_{\rm P}(t) = 0$. In this way, we obtain from Eqs. (36) and (37) that the steady-state values $\langle\sigma_{01}^{(s)}\rangle$ and $\langle\sigma_{02}^{(s)}\rangle$ are zero, i.e.,

$$\langle\sigma_{01}^{(s)}\rangle = \langle\sigma_{02}^{(s)}\rangle = 0. \quad (42)$$

The steady-state values $\langle\sigma_{12}^{(s)}\rangle$ and $\langle\sigma_{ll}^{(s)}\rangle$ $(l=0,1,2)$ can be obtained via Eqs. (38)–(41). However, in the usual experiments with SFQCs, the condition $k_{\rm B}T \ll |E_i - E_j|$ $(i,j=0,1,2, i\neq j)$ is fulfilled. Thus, the population of the energy levels $|1\rangle$ and $|2\rangle$ due to thermal excitations can be neglected, and the steady-state values $\langle\sigma_{12}^{(s)}\rangle$ and $\langle\sigma_{ll}^{(s)}\rangle$ $(l=0,1,2)$ can be approximately given as

$$\langle\sigma_{12}^{(s)}\rangle \approx \langle\sigma_{11}^{(s)}\rangle \approx \langle\sigma_{22}^{(s)}\rangle \approx 0, \text{ and } \langle\sigma_{00}^{(s)}\rangle \approx 1. \quad (43)$$

By numerically solving Eqs. (38)–(41), we find that $|\langle\sigma_{12}^{(s)}\rangle| < 10^{-2}$ and $\langle\sigma_{ll}^{(s)}\rangle < 3\times10^{-2}$ $(l=1,2)$ with the parameters used in following discussions on numerical calculations. Thus, the approximation in Eq. (43) is reasonable.

D. Formal solution of quantum Langevin equations

The time-dependent average values $\langle\sigma_{lm}(t)\rangle$ can be obtained by solving the equations for the average values $\langle\sigma_{lm}\rangle$ using the Fourier transform. Because we are only interested in the linear magnetic susceptibility of the three-level system to the probe field $\Phi_{\rm P}(t)$, the solutions are only calculated to first order in $\Phi_{\rm P}(t)$. Therefore, here we first transform Eqs. (36)–(41) into equations for the average values $\langle\sigma_{lm}\rangle$, and afterwards, in the terms including $\Phi_{\rm P}(t)$, we replace all the average values $\langle\sigma_{lm}(t)\rangle$ by their steady-state values $\langle\sigma_{lm}^{(s)}\rangle$.

As shown in Eq. (42), the steady-state values $\langle\sigma_{01}^{(s)}\rangle$ and $\langle\sigma_{02}^{(s)}\rangle$ are zero, thus, the time-dependent average values $\langle\sigma_{12}(t)\rangle$ and $\langle\sigma_{ll}(t)\rangle$ $(l=0,1,2)$ are independent of $\Phi_{\rm P}(t)$ when calculated to first order in $\Phi_{\rm P}(t)$, and do not affect the linear magnetic susceptibility of the three-level SFQC. Therefore, we only need to calculate the time-dependent average values $\langle\sigma_{01}(t)\rangle$ and $\langle\sigma_{02}(t)\rangle$. The formal solutions of the average values $\langle\sigma_{01}(t)\rangle$ and $\langle\sigma_{02}(t)\rangle$ are expressed as

$$\langle\sigma_{01}(t)\rangle = i\frac{I_{10}}{\hbar}\int dt' G_{22}(\tau)\Phi_{\rm P}(t')e^{i\omega_1 t'} - i\frac{I_{20}}{\hbar}\int dt' G_{12}(\tau)\Phi_{\rm P}(t')e^{i\omega' t'} + G_{22}(t)\langle\sigma_{01}(0)\rangle - G_{12}(t)\langle\sigma_{02}(0)\rangle, \quad (44)$$

$$\langle\sigma_{02}(t)\rangle = i\frac{I_{20}}{\hbar}\int dt' G_{11}(\tau)\Phi_{\rm P}(t')e^{i\omega' t'} - i\frac{I_{10}}{\hbar}\int dt' G_{21}(\tau)\Phi_{\rm P}(t')e^{i\omega_1 t'} - G_{21}(t)\langle\sigma_{01}(0)\rangle + G_{22}(t)\langle\sigma_{02}(0)\rangle. \quad (45)$$

The Fourier transforms of the Green's functions $G_{lm}(\tau)$ in Eqs. (44) and (45), are given by

$$G_{11}(\omega) = \int d\tau\, G_{11}(\tau)\, e^{i\omega\tau} = \frac{i\,(\omega + \Gamma_{11})}{D(\omega)}, \tag{46}$$

$$G_{12}(\omega) = \int d\tau\, G_{12}(\tau)\, e^{i\omega\tau} = \frac{i\,(\Gamma_{12} - \Omega_{\rm D})}{D(\omega)}, \tag{47}$$

$$G_{21}(\omega) = \int d\tau\, G_{21}(\tau)\, e^{i\omega\tau} = \frac{i(\Gamma_{21} - \Omega_{\rm D}^{*})}{D(\omega)}, \tag{48}$$

$$G_{22}(\omega) = \int d\tau\, G_{22}(\tau)\, e^{i\omega\tau} = \frac{i\,(\omega - \Delta + \Gamma_{22})}{D(\omega)}, \tag{49}$$

with the denominator

$$D(\omega) = -(\omega + \Gamma_{11})(\omega - \Delta + \Gamma_{22}) + (\Gamma_{12} - \Omega_{\rm D})\left(\Gamma_{21} - \Omega_{\rm D}^{*}\right). \tag{50}$$

E. Discussions on decay rates

The complex coefficients Γ_{lm} in Eqs. (36)–(41) incorporate the effects of the environment on the three-level SFQC. The real parts of Γ_{lm} represent the Lamb frequency shifts of the three-level SFQC, while the imaginary parts of Γ_{lm} represent the damping rates of the three-level SFQC.

We can further simplify Γ_{lm} via the fluctuation-dissipation theorem. According to the fluctuation-dissipation theorem, the spectral density $S(\omega)$ in Eq. (27) and the imaginary part of the environmental susceptibility $\chi''(\omega)$ in Eq. (22) satisfy the following relation:

$$S(\omega) = \chi''(\omega)\coth\left(\frac{\hbar\omega}{2k_{\rm B}T}\right). \tag{51}$$

Here, T is the equilibrium temperature of the environment. In our calculations, $\chi''(\omega)$ is approximately given by an Ohmic spectrum with exponential cutoff [72,73]

$$\chi''(\omega) = \eta\,\omega\exp\left(-\frac{|\omega|}{\omega_c}\right). \tag{52}$$

Here, ω_c is the cutoff frequency typically assumed to be much larger than all the other relevant frequency scales of the three-level SFQC. The dimensionless constants $\eta|I_{ij}|^2/2\pi$ $(i, j = 0, 1, 2)$ represent the coupling strengths between the three-level SFQC and its environment.

Using Eqs. (23), (29), (51), and (52), we can simplify all formulas related to $\chi(\omega)$ and $\widetilde{S}(\omega)$ by $\chi''(\omega)$. In the following calculations, we neglect the real parts of the complex coefficients Γ_{lm}, which are responsible for the Lamb frequency shifts of the three-level SFQC. In this way, all the complex coefficients Γ_{lm} are replaced by $i\gamma_{lm}$, with $\gamma_{lm} = {\rm Im}(\Gamma_{lm})$.

In principle, γ_{lm} $(l, m = 1, 2)$ can be calculated numerically from the expressions of Γ_{lm} $(l, m = 1, 2)$ given in Appendix B. In Fig. 3, we plot the damping rates γ_{lm} $(l, m = 1, 2)$ as functions of f, T, and $|\Omega_{\rm D}|$ with the parameters given in Appendix C. We find in Fig. 3(a) that the damping rate γ_{11} reaches its maximum at the optimal point and decreases as f deviates from 0.5 when the environmental equilibrium temperature $T = 0$. However, when $T \neq 0$, the damping rate γ_{11} reaches its minimum at the optimal point. As f deviates from 0.5, γ_{11} first increases, and then decreases after reaching its maximum point. We find in Fig. 3(a) that the damping rate γ_{22} reaches its minimum at the optimal point. As f deviates from 0.5, γ_{22} first increases, and then decreases after reaching its maximum point. In Fig. 3(b), we find that the damping rates γ_{11} and γ_{22} increase when the environmental equilibrium temperature T goes up. In Figs. 3(c) and 3(d), we find that γ_{11} and γ_{22} are almost not affected by the Rabi frequency $|\Omega_{\rm D}|$. Whereas in Figs. 3(e) and 3(f), we find that γ_{12} and γ_{12} are almost linearly dependent on the Rabi frequency $|\Omega_{\rm D}|$.

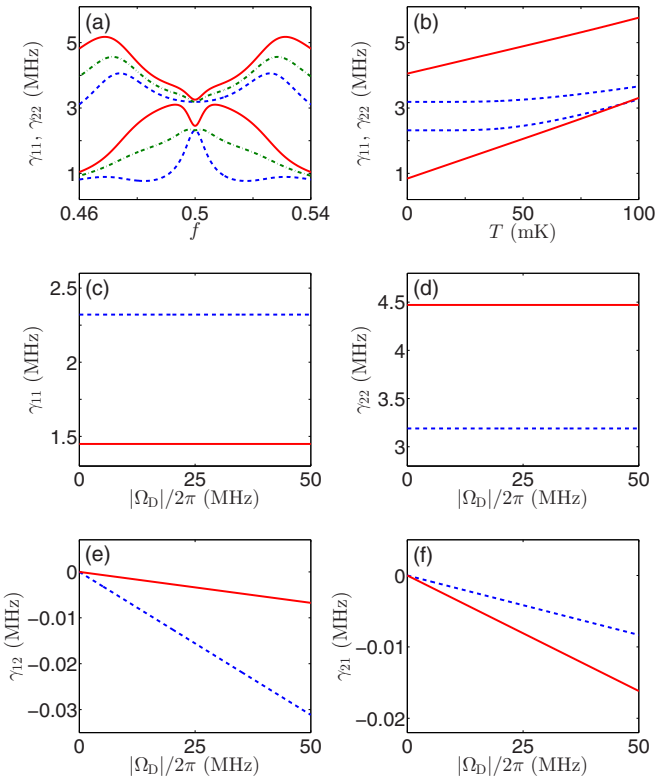

FIG. 3. (Color online) Damping rates γ_{11} (the three lowest curves) and γ_{22} (the three highest curves) in (a) as functions of the reduced magnetic flux f, are plotted for the temperatures $T = 0$ (blue dashed curves), $T = 25$ mK (green dashed-dotted curves), and $T = 50$ mK (red solid curves). Damping rates γ_{11} (the two lowest curves) and γ_{22} (the two highest curves) in (b) as functions of the temperature T, are plotted for the reduced magnetic flux $f = 0.5$ (blue dashed curves) and $f = 0.525$ (red solid curves). Damping rates γ_{11} in (c), γ_{22} in (d), γ_{12} in (e), and γ_{21} in (f) as functions of the Rabi frequency $|\Omega_{\rm D}|$, are plotted for the reduced magnetic flux $f = 0.5$ (blue dashed curve) and $f = 0.525$ (red solid curve). Here, Δ is assumed to be 0. In (a) and (b), $|\Omega_{\rm D}|$ is assumed to be 0. In (e) and (f), T is assumed to be 25 mK. The other parameters of the three-level SFQC are provided in Appendix C.

F. Comparison between the quantum Langevin equation and the Lindblad master equation

Now, we make a comparison between the quantum Langevin equations in Eqs. (36)–(41) with the Lindblad master equation. The method for deriving the quantum Langevin equations in Eqs. (36)–(41) is similar to that in Ref. [74]

for deriving the Lindblad master equation with the Born-Markov approximation and the RWA. And, we can transform the quantum Langevin equations in Eqs. (36)–(41) into an equivalent Lindblad master equation [74]. However, there are differences between the quantum Langevin equations in Eqs. (36)–(41) and the commonly used type of Lindblad master equations.

(i) Usually, a commonly used type of Lindblad master equation (denoted by cLME), e.g., the Lindblad master equation used in Ref. [50], does not consider the effects of the driving field on the coupling between the three-level SFQC and its environment. That is to say, the frequency shifts and the damping rates induced by the environment in the cLME are independent of the driving field. However, in this paper we take these effects of the driving field into account as in Ref. [69] and derive the driving-field-dependent complex coefficients Γ_{lm} (see Appendix B).

(ii) When the driving field $\Phi_{\rm D}$ is not applied, the real (imaginary) parts of the complex coefficients Γ_{lm} are equivalent to the frequency shifts (the damping rates) in the cLME. For example, γ_{11} and γ_{22}, the imaginary parts of Γ_{11} and Γ_{22}, are equivalent to the damping rates of the off-diagonal matrix elements ρ_{21} and ρ_{31} in Ref. [50], respectively. However, when the driving field $\Phi_{\rm D}$ is applied, the complex coefficients Γ_{lm} are modified by the Rabi frequency $|\Omega_{\rm D}|$ and the detuning Δ of the driving field $\Phi_{\rm D}$. In addition, some of the complex coefficients Γ_{lm}, e.g., Γ_{12} and Γ_{21}, are not considered in the cLME because these are nonzero only when the driving field $\Phi_{\rm D}$ is applied. Thus, the phenomena induced by these complex coefficients Γ_{lm}, e.g., Γ_{12} and Γ_{21}, can not be explained by using the cLME. In Sec. IV, we will show that γ_{12} and γ_{21}, the imaginary parts of Γ_{12} and Γ_{21}, can make the two peaks in the absorption spectrum for ATS have different heights.

IV. MAGNETIC SUSCEPTIBILITY

To study the linear response of the three-level SFQC to the probe field when the three-level SFQC is in the steady state, we now calculate the linear magnetic susceptibilities.

A. Susceptibility of the three-level SFQC

The magnetic susceptibility $\chi_q(\omega)$ can be given by the Fourier transform of Eq. (13) as

$$\chi_q(\omega)=\int d\tau_1\left\langle\frac{\delta\hat{I}(t)}{\delta\Phi_{\rm P}(t_1)}\right\rangle\exp(i\omega\tau_1), \tag{53}$$

with the time interval $\tau_1=t-t_1$. In the rotating reference frame, the loop current operator $\hat{I}(t)$ in Eq. (53) takes the form as shown in Eq. (17),

$$\hat{I}(t)=[I_{01}\sigma_{01}(t)e^{-i\omega_1 t}+I_{02}\sigma_{02}(t)e^{-i\omega' t}+I_{12}\sigma_{12}(t)e^{-i\omega_0 t}+\text{H.c.}]+\sum_{i=0}^{2}I_{ii}\sigma_{ii}(t). \tag{54}$$

As discussed in Sec. III D, the average values $\langle\sigma_{12}(t)\rangle$ and $\langle\sigma_{ll}(t)\rangle$ ($l=0,1,2$) are independent of $\Phi_{\rm P}(t)$, and do not affect the magnetic susceptibility $\chi_q(\omega)$. Thus, the susceptibility $\chi_q(\omega)$ defined in Eq. (53) can be calculated via the functional derivatives of the average values $\langle\sigma_{01}(t)\rangle$, $\langle\sigma_{02}(t)\rangle$, $\langle\sigma_{10}(t)\rangle$, and $\langle\sigma_{20}(t)\rangle$ over the probe field $\Phi_{\rm P}(t_1)$. Using Eqs. (44) and (45), the functional derivatives of the average values $\langle\sigma_{01}(t)\rangle$ and $\langle\sigma_{02}(t)\rangle$ over the probe field $\Phi_{\rm P}(t_1)$ can be given as

$$\frac{\delta\langle\sigma_{01}(t)\rangle}{\delta\Phi_{\rm P}(t_1)}=i\frac{I_{10}}{\hbar}G_{22}(\tau_1)e^{i\omega_1 t_1}-i\frac{I_{20}}{\hbar}G_{12}(\tau_1)e^{i\omega' t_1}, \tag{55}$$

$$\frac{\delta\langle\sigma_{02}(t)\rangle}{\delta\Phi_{\rm P}(t_1)}=i\frac{I_{20}}{\hbar}G_{11}(\tau_1)e^{i\omega' t_1}-i\frac{I_{10}}{\hbar}G_{21}(\tau_1)e^{i\omega_1 t_1}. \tag{56}$$

The functional derivatives of the average values $\langle\sigma_{10}(t)\rangle$ and $\langle\sigma_{20}(t)\rangle$ over the probe field $\Phi_{\rm P}(t_1)$ can be obtained by taking the conjugates of Eqs. (55) and (56). Therefore, we can straightforwardly obtain

$$\chi_q(\omega)=\chi_{01}(\omega)+\chi_{02}(\omega). \tag{57}$$

Here, $\chi_{01}(\omega)$ and $\chi_{02}(\omega)$ are determined by

$$\chi_{01}(\omega)=\int d\tau_1\left\langle\frac{\delta[I_{01}\sigma_{01}(t)e^{-i\omega_1 t}+\text{H.c.}]}{\delta\Phi_{\rm P}(t_1)}\right\rangle e^{i\omega\tau_1}, \tag{58}$$

$$\chi_{02}(\omega)=\int d\tau_1\left\langle\frac{\delta[I_{02}\sigma_{02}(t)e^{-i\omega' t}+\text{H.c.}]}{\delta\Phi_{\rm P}(t_1)}\right\rangle e^{i\omega\tau_1}. \tag{59}$$

According to Eqs. (58) and (59), using Eqs. (46)–(49), (55), and (56), we can obtain

$$\chi_{01}(\omega)=\frac{\alpha_{01}(\delta_1-\Delta+i\gamma_{22})}{D_1(\delta_1)}, \tag{60}$$

$$\chi_{02}(\omega)=\frac{\alpha_{02}(\delta_2+i\gamma_{11})}{D_1(\delta_2)}. \tag{61}$$

Here, $\alpha_{0i}=|I_{0i}|^2/\hbar$ $(i=1,2)$, $\delta_1=\omega-\omega_1$, $\delta_2=\omega-\omega'$, and

$$D_1(\omega)=-(\omega+i\gamma_{11})(\omega-\Delta+i\gamma_{22})+(i\gamma_{12}-\Omega_{\rm D})(i\gamma_{21}-\Omega_{\rm D}^*). \tag{62}$$

We can observe from Eqs. (58) and (59) that the magnetic susceptibility $\chi_{01}(\omega)$ and $\chi_{02}(\omega)$ are odd functions of the frequency ω, thus we only need to study the behavior of these magnetic susceptibilities in the regime $\omega>0$. In this case, the functional derivatives of the average values $\langle\sigma_{10}(t)\rangle$ and $\langle\sigma_{20}(t)\rangle$ over the probe field $\Phi_{\rm P}(t_1)$ are neglected in obtaining Eqs. (60) and (61) because these functional derivatives are responsible for small antirotating wave terms when $\omega>0$. We have also neglected all fast-oscillating terms, e.g., the second term in Eq. (55), in obtaining Eqs. (60) and (61). These fast-oscillating terms account for the three-wave mixing phenomenon of the three-level SFQC, which is not in the scope of this paper.

The magnetic susceptibility $\chi_q(\omega)$ in Eq. (57) consists of two terms: $\chi_{01}(\omega)$ and $\chi_{02}(\omega)$. $\chi_{01}(\omega)$ results from the $|0\rangle\leftrightarrow|1\rangle$ transition induced by the probe field, while $\chi_{02}(\omega)$ results from the $|0\rangle\leftrightarrow|2\rangle$ transition induced by the probe field. From Eqs. (60) and (61), we can find that $\chi_{01}(\omega)$ and $\chi_{02}(\omega)$ are similar to the susceptibilities of three-level natural atoms [40,76], driven at the $|1\rangle\leftrightarrow|2\rangle$ transition by a strong field, and probed by a weak field. Here, $\chi_{01}(\omega)$ [or $\chi_{02}(\omega)$] is similar to the susceptibility of three-level natural atoms with ladder-type (or Λ-type) transitions, because in such natural

atoms the weak probe field can induce the $|0\rangle \leftrightarrow |1\rangle$ ($|0\rangle \leftrightarrow |2\rangle$) transition, but cannot induce the $|0\rangle \leftrightarrow |2\rangle$ ($|0\rangle \leftrightarrow |1\rangle$) transition.

In this study, we assume that the Rabi frequency $|\Omega_D|$, the driving-field detuning Δ, and the damping rates γ_{ij} ($i, j = 1, 2$) are all much smaller than the transition frequencies ω_i ($i = 1, 2, 3$). With these assumptions, we can find that $\chi_{01}(\omega)$ plays a major role in the magnetic susceptibility $\chi_q(\omega)$ when ω is near resonant to the $|0\rangle \leftrightarrow |1\rangle$ transition, i.e., $\chi_q(\omega) \approx \chi_{01}(\omega)$ when $\omega \approx \omega_1$. In contrast, $\chi_{02}(\omega)$ plays a major role in the magnetic susceptibility $\chi_q(\omega)$ when ω is near resonant to the $|0\rangle \leftrightarrow |2\rangle$ transition, i.e., $\chi_q(\omega) \approx \chi_{02}(\omega)$ when $\omega \approx \omega_2$. Hereafter, we denote the frequency range, in which ω is near resonant to the $|0\rangle \leftrightarrow |1\rangle$ (or $|0\rangle \leftrightarrow |2\rangle$) transition, as the $|0\rangle \leftrightarrow |1\rangle$ (or $|0\rangle \leftrightarrow |2\rangle$) frequency range.

As shown in Fig. 2(b), the moduli of the loop current transition matrix elements $|I_{01}|$ and $|I_{02}|$ are dependent on the bias magnetic flux. Thus, we can find from Eqs. (57), (60), and (61) that the magnetic susceptibility $\chi_q(\omega)$ can be tuned by the bias magnetic flux through $|I_{01}|$ and $|I_{02}|$. According to the symmetric analysis [27], when the bias magnetic flux is at the optimal point, $|I_{02}| = 0$ and the probe field $\Phi_P(t)$ can not induce the $|0\rangle \leftrightarrow |2\rangle$ transition of the three-level SFQC. At this special point, $\chi_q(\omega)$ has the same function as $\chi_{01}(\omega)$, thus, the three-level SFQC can respond to the probe field in the $|0\rangle \leftrightarrow |1\rangle$ frequency range, like natural atoms with ladder-type transitions. However, when the bias magnetic flux deviates from the optimal point, the probe field $\Phi_P(t)$ can induce both the $|0\rangle \leftrightarrow |1\rangle$ and $|0\rangle \leftrightarrow |2\rangle$ transitions via interactions with the loop current of the SFQC. In this case, $\chi_q(\omega)$ is the summation of $\chi_{01}(\omega)$ and $\chi_{02}(\omega)$. Thus, the three-level SFQC can respond to the probe field in both the $|0\rangle \leftrightarrow |1\rangle$ and $|0\rangle \leftrightarrow |2\rangle$ frequency ranges. In other words, the three-level SFQC acts like a combination of natural atoms with ladder-type transitions and natural atoms with Λ-type transitions. This is an obvious difference between the linear responses of three-level SFQCs and three-level natural atoms.

B. Conditions for realizing EIT and ATS

We know that the linear response of the driven three-level SFQC to the probe field can be used to characterize EIT and ATS. Let us now study the conditions for realizing EIT and ATS in the three-level SFQC. As discussed in Sec. IV A, the three-level SFQC may respond to the probe field in two different frequency ranges: the $|0\rangle \leftrightarrow |1\rangle$ frequency range and the $|0\rangle \leftrightarrow |2\rangle$ frequency range. Thus, EIT (ATS) may occur in these two frequency ranges. In the $|0\rangle \leftrightarrow |1\rangle$ frequency range, the EIT (ATS) spectrum is characterized by $\chi_{01}(\omega)$, while in the $|0\rangle \leftrightarrow |2\rangle$ frequency range, the EIT (ATS) spectrum is characterized by $\chi_{02}(\omega)$. We first introduce the method provided in Refs. [51,75,76] of distinguishing EIT from ATS. Then, we combine this method with other necessary conditions to derive the conditions for realizing EIT and ATS.

References [51,75,76] provided a method of distinguishing EIT from ATS by decomposing the linear response of a three-level quantum system into two resonances. For example, the magnetic susceptibilities $\chi_{01}(\omega)$ and $\chi_{02}(\omega)$ can be decomposed as

$$\begin{aligned}\chi_{01}(\omega) &= R_+^{(01)}(\delta_1) + R_-^{(01)}(\delta_1) \\ &= \frac{\alpha_{01}}{\delta_- - \delta_+}\frac{\delta_+ - \Delta + i\gamma_{22}}{\delta_1 - \delta_+} \\ &\quad + \frac{\alpha_{01}}{\delta_+ - \delta_-}\frac{\delta_- - \Delta + i\gamma_{22}}{\delta_1 - \delta_-},\end{aligned} \tag{63}$$

$$\begin{aligned}\chi_{02}(\omega) &= R_+^{(02)}(\delta_2) + R_-^{(02)}(\delta_2) \\ &= \frac{\alpha_{02}}{\delta_- - \delta_+}\frac{\delta_+ + i\gamma_{11}}{\delta_2 - \delta_+} \\ &\quad + \frac{\alpha_{02}}{\delta_+ - \delta_-}\frac{\delta_- + i\gamma_{11}}{\delta_2 - \delta_-},\end{aligned} \tag{64}$$

where $\delta_\pm$ are the complex roots of the equation $D_1(\delta) = 0$. If the driving-field detuning Δ is assumed to be zero and the damping rates γ_{12} and γ_{21} are neglected, then $\delta_\pm$ can be given by

$$\delta_\pm = \tfrac{1}{2}\left(-i\gamma_{11} - i\gamma_{22} \pm \Omega_T\right), \tag{65}$$

with $\Omega_T = \sqrt{4|\Omega_D|^2 - (\gamma_{11} - \gamma_{22})^2}$. For simplicity, the following discussions for EIT and ATS will first be limited to the case that $\Delta = 0$ and $\gamma_{12} = \gamma_{21} = 0$. The effects of nonzero Δ, γ_{12}, and γ_{21} will be discussed in Sec. IV D.

We first study the realization of EIT (ATS) in the $|0\rangle \leftrightarrow |1\rangle$ frequency range, where the EIT (ATS) spectrum is characterized by $\chi_{01}(\omega)$. According to Refs. [51,75,76], EIT and ATS occur in two different driving regimes, respectively, defined by the relation between the Rabi frequency $|\Omega_D|$ and the threshold $|\gamma_{11} - \gamma_{22}|/2$. EIT can only occur in the regime $|\Omega_D| < |\gamma_{11} - \gamma_{22}|/2$, which is called here the weak-driving regime, while ATS can only occur in the regime $|\Omega_D| > |\gamma_{11} - \gamma_{22}|/2$, which is called here the strong-driving regime. The two resonances $R_\pm^{(01)}(\delta_1)$ of $\chi_{01}(\omega)$ have different shapes in these two driving regimes: (i) In the weak-driving regime, $\mathrm{Re}(\delta_\pm) = 0$, and then $\mathrm{Im}[R_+^{(01)}(\delta_1)]$ and $\mathrm{Im}[R_-^{(01)}(\delta_1)]$ are two Lorentzians with different signs, both centered at $\delta_1 = 0$. (ii) In the strong-driving regime, $\mathrm{Re}(\delta_+) = -\mathrm{Re}(\delta_-) \neq 0$ and $\mathrm{Im}(\delta_+) = \mathrm{Im}(\delta_-)$, and then $\mathrm{Im}[R_+^{(01)}(\delta_1)]$ and $\mathrm{Im}[R_-^{(01)}(\delta_1)]$ are two positive peaks located at $\delta_1 = \pm\Omega_T/2$, respectively. When $|\Omega_D| \gg |\gamma_{11} - \gamma_{22}|/2$, $\mathrm{Im}[R_+^{(01)}(\delta_1)]$ and $\mathrm{Im}[R_-^{(01)}(\delta_1)]$ are approximately two positive Lorentzians centered at $\delta_1 = \pm|\Omega_D|$, respectively. The bifurcation point $|\Omega_D| = |\gamma_{11} - \gamma_{22}|/2$ is a special case where the decomposition in Eq. (63) is invalid. In this study, we do not consider the conditions for realizing EIT and ATS at this bifurcation point.

The conditions $|\Omega_D| < |\gamma_{11} - \gamma_{22}|/2$ and $|\Omega_D| > |\gamma_{11} - \gamma_{22}|/2$ can be used to distinguish EIT from ATS in the $|0\rangle \leftrightarrow |1\rangle$ frequency range, however, these are not the sufficient conditions for the realization of EIT (ATS). The dip in the absorption spectrum of EIT (ATS) implies that the resonant point $\mathrm{Im}[\chi_{01}(\omega_1)]$ must be a local minimum when EIT (ATS) is realized. By analyzing the derivative of $\mathrm{Im}[\chi_{01}(\omega)]$ over ω, we find that $\mathrm{Im}[\chi_{01}(\omega_1)]$ is the local minimum if $|\Omega_D| > \gamma_{22}\sqrt{\gamma_{22}/(\gamma_{11} + 2\gamma_{22})}$. Combining this condition with $|\Omega_D| < |\gamma_{11} - \gamma_{22}|/2$ ($|\Omega_D| > |\gamma_{11} - \gamma_{22}|/2$), we finally obtain the

condition for realizing EIT (ATS) in the $|0\rangle \leftrightarrow |1\rangle$ frequency range:

$$\text{EIT}: \begin{cases} \gamma_{11} > 2\gamma_{22}, \\ |\Omega_D| > \gamma_{22}\sqrt{\frac{\gamma_{22}}{\gamma_{11}+2\gamma_{22}}}, \\ |\Omega_D| < \frac{|\gamma_{11}-\gamma_{22}|}{2}, \end{cases} \tag{66}$$

$$\text{ATS}: \begin{cases} |\Omega_D| > \frac{|\gamma_{11}-\gamma_{22}|}{2}, & \gamma_{11} > 2\gamma_{22} \\ |\Omega_D| > \gamma_{22}\sqrt{\frac{\gamma_{22}}{\gamma_{11}+2\gamma_{22}}}, & \gamma_{11} \leqslant 2\gamma_{22}. \end{cases} \tag{67}$$

The above discussions can also be applied to the $|0\rangle \leftrightarrow |2\rangle$ frequency range. Considering that the damping rates γ_{11} and γ_{22} play different roles in the expressions for $\chi_{01}(\omega)$ and $\chi_{02}(\omega)$ in Eqs. (60) and (61), the conditions for realizing EIT (ATS) in the $|0\rangle \leftrightarrow |2\rangle$ frequency range are

$$\text{EIT}: \begin{cases} \gamma_{22} > 2\gamma_{11}, \\ |\Omega_D| > \gamma_{11}\sqrt{\frac{\gamma_{11}}{\gamma_{22}+2\gamma_{11}}}, \\ |\Omega_D| < \frac{|\gamma_{11}-\gamma_{22}|}{2}, \end{cases} \tag{68}$$

$$\text{ATS}: \begin{cases} |\Omega_D| > \frac{|\gamma_{11}-\gamma_{22}|}{2}, & \gamma_{22} > 2\gamma_{11} \\ |\Omega_D| > \gamma_{11}\sqrt{\frac{\gamma_{11}}{\gamma_{22}+2\gamma_{11}}}, & \gamma_{22} \leqslant 2\gamma_{11}. \end{cases} \tag{69}$$

C. EIT and ATS regimes

Here, we introduce two reduced parameters γ_R and Ω_R to better interpret the conditions in Eqs. (66)–(69). Using γ_R and Ω_R, the reduced magnetic susceptibility becomes

$$\begin{aligned} \chi_R(\delta_R) &= \chi_R'(\delta_R) + i\chi_R''(\delta_R) \\ &= \frac{\delta_R + i\gamma_R}{\Omega_R^2 - (\delta_R + i)(\delta_R + i\gamma_R)}. \end{aligned} \tag{70}$$

The reduced magnetic susceptibility $\chi_R(\delta_R)$ can also be decomposed into two resonances as in Eqs. (63) and (64),

$$\begin{aligned} \chi_R(\delta_R) &= R_+(\delta_R) + R_-(\delta_R) \\ &= \frac{\delta_+^{(R)} + i\gamma_R}{(\delta_-^{(R)} - \delta_+^{(R)})(\delta_R - \delta_+^{(R)})} \\ &\quad + \frac{\delta_-^{(R)} + i\gamma_R}{(\delta_+^{(R)} - \delta_-^{(R)})(\delta_R - \delta_-^{(R)})}, \end{aligned} \tag{71}$$

with

$$\delta_\pm^{(R)} = \tfrac{1}{2}[-i(1+\gamma_R) \pm \sqrt{4|\Omega_R|^2 - (1-\gamma_R)^2}]. \tag{72}$$

Any certain set of parameters of the SFQC $(\gamma_{11}, \gamma_{22}, |\Omega_D|)$ can be transformed into a point (γ_R, Ω_R) in the γ_R-Ω_R plane, with a corresponding reduced magnetic susceptibility $\chi_R(\delta_R)$ defined in Eq. (70). The transformation relation depends on the explicit expression of the magnetic susceptibility, i.e., $\chi_{01}(\omega)$ or $\chi_{02}(\omega)$. For $\chi_{01}(\omega)$, the transformation relation is $\gamma_R = \gamma_{22}/\gamma_{11}$, $\Omega_R = |\Omega_D|/\gamma_{11}$, and $\chi_R(\delta_R) = \gamma_{11}\chi_{01}(\gamma_{11}\delta_R + \omega_1)/\alpha_{01}$. While for $\chi_{02}(\omega)$, $\gamma_R = \gamma_{11}/\gamma_{22}$, $\Omega_R = |\Omega_D|/\gamma_{22}$, and $\chi_R(\delta_R) = \gamma_{22}\chi_{02}(\gamma_{22}\delta_R + \omega')/\alpha_{02}$. We note that after the transformation, $\chi_R(\delta_R)$ still keeps all the characteristics of the susceptibility $\chi_{01}(\omega)$ [$\chi_{02}(\omega)$] we need to study EIT and ATS. Thus, using γ_R and Ω_R, we can rewrite the conditions in Eqs. (66)–(69) into a unified form

$$\text{EIT}: \begin{cases} \gamma_R < \frac{1}{2}, \\ \Omega_R > \Omega_M(\gamma_R), \\ \Omega_R < \Omega_W(\gamma_R), \end{cases} \tag{73}$$

$$\text{ATS}: \begin{cases} \Omega_R > \Omega_W(\gamma_R), & \gamma_R < \frac{1}{2} \\ \Omega_R > \Omega_M(\gamma_R), & \gamma_R \geqslant \frac{1}{2} \end{cases} \tag{74}$$

with the threshold functions defined as

$$\Omega_W(\gamma_R) = \frac{|1-\gamma_R|}{2}, \tag{75}$$

$$\Omega_M(\gamma_R) = \gamma_R\sqrt{\frac{\gamma_R}{1+2\gamma_R}}. \tag{76}$$

In the first quadrant of the γ_R-Ω_R plane, the points (γ_R, Ω_R) which fulfill the condition for realizing EIT (ATS) comprise the EIT (ATS) regime. The borders of the EIT and ATS regimes are defined by $\Omega_W(\gamma_R)$ and $\Omega_M(\gamma_R)$. In Fig. 4, we plot $\Omega_W(\gamma_R)$ (black dashed-dotted curve) and $\Omega_M(\gamma_R)$ (black solid curve) in the first quadrant of the γ_R-Ω_R plane. $\Omega_W(\gamma_R)$ is the reduced form of the threshold $|\gamma_{11} - \gamma_{22}|/2$ mentioned above, which separates the quadrant into the weak-driving (area below the black dashed curve) and the strong-driving (area above the black dashed curve) regimes. While $\Omega_M(\gamma_R)$ describes the characteristic of the resonant point $\chi_R''(0)$, $\Omega_M(\gamma_R)$ also separates the quadrant into two regimes. In Fig. 4, the area above the black solid curve is the minimum regime. In this regime, the resonant point $\chi_R''(0)$ is a local minimum of $\chi_R''(\delta_R)$. By contrast, the left part of the quadrant, which includes the area below the black solid curve and the black solid curve

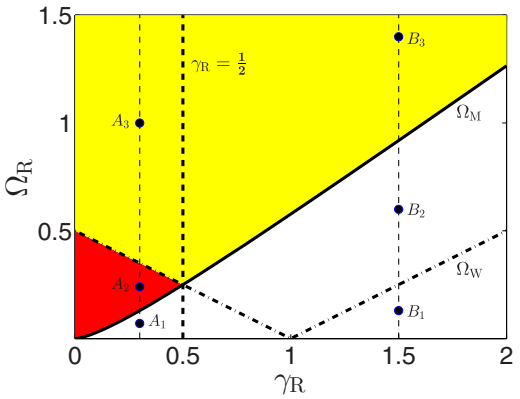

FIG. 4. (Color online) Thresholds Ω_W (dashed-dotted curve) and Ω_M (solid curve) are plotted as functions of γ_R. The red (yellow) area represents the EIT (ATS) regime. Six representative points $A_1(0.3,0.07)$, $A_2(0.3,0.24)$, $A_3(0.3,1)$, $B_1(1.5,0.13)$, $B_2(1.5,0.6)$, and $B_3(1.5,1.4)$ are marked by round dots.

itself, is the maximum regime. In this regime, the resonant point $\chi_R''(0)$ is a local maximum of $\chi_R''(\delta_R)$.

According to the conditions in Eqs. (73) and (74), the EIT regime (red area in Fig. 4) is the area where the weak-driving regime and the minimum regime overlaps. In contrast, the ATS regime (yellow area in Fig. 4) is the area where the strong-driving regime and the minimum regime overlap.

In Fig. 4, we find that the line $\gamma_R = \frac{1}{2}$ divides the quadrant into two distinct areas. EIT can only be realized in the area where $\gamma_R < \frac{1}{2}$. And in this area, for a given γ_R, a transition from EIT to ATS can be realized when increasing Ω_R. We take three points A_1–A_3 as examples and plot the corresponding $\chi_R''(\delta_R)$ and $\mathrm{Im}[R_\pm(\delta_R)]$ in Figs. 5(a)–5(c), respectively. In Fig. 4, A_1 lies below both curves Ω_W and Ω_M. Thus, in Fig. 5(a), two Lorentzians $\mathrm{Im}[R_\pm(\delta_R)]$ are centered at $\delta_R = 0$ with different signs, but their summation $\chi_R''(\delta_R)$ does not exhibit a dip. A_2 lies below the curve Ω_W and above the curve Ω_M, just in the EIT regime. Thus, in Fig. 5(b), the interference between the two Lorentzians $\mathrm{Im}[R_\pm(\delta_R)]$ is strong enough to make a dip appear in $\chi_R''(\delta_R)$. As for A_3, this point lies above both curves Ω_W and Ω_M, i.e., in the ATS regime. Thus, in Fig. 5(c), $\mathrm{Im}[R_\pm(\delta_R)]$ are two positive peaks located in different positions, and the gap between them makes a dip appear in $\chi_R''(\delta_R)$.

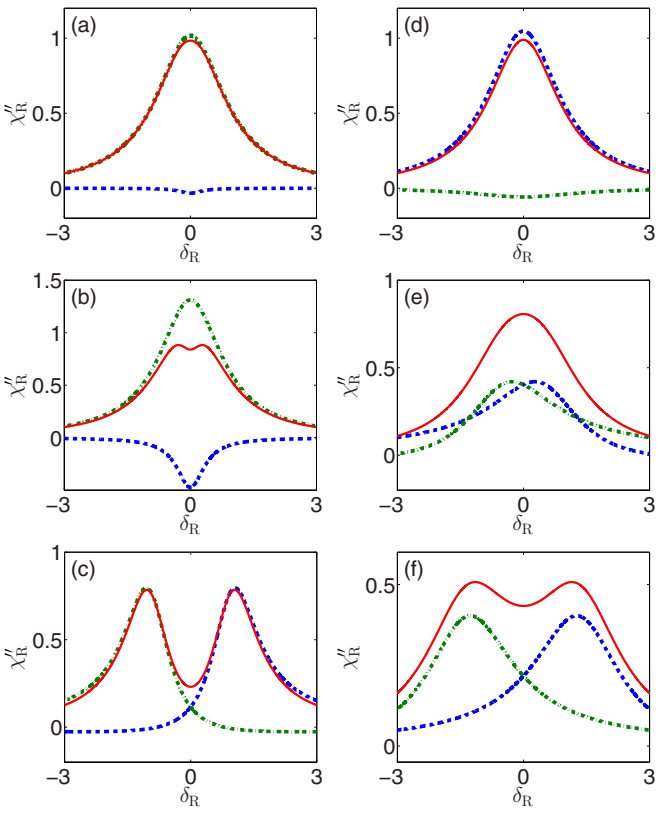

FIG. 5. (Color online) Imaginary parts of the reduced magnetic susceptibility $\chi_R''(\delta_R)$ (red solid curve), the resonances $\mathrm{Im}[R_+(\delta_R)]$ (blue dashed curve), and $\mathrm{Im}[R_-(\delta_R)]$ (green dashed-dotted curve) are plotted. Figures (a)–(c) correspond with the points A_1–A_3 in Fig. 4, respectively. While figures (d)–(f) correspond with the points B_1–B_3 in Fig. 4, respectively.

TABLE I. EIT and ATS experiments in SQCs and natural atoms.

Experiments	Systems	Susceptibility	γ_R
Ref. [49]	SQCs	$\chi_{01}(\omega)$	1.93
Ref. [50]	SQCs	$\chi_{01}(\omega)$	0.96
Ref. [53]	SQCs	$\chi_{01}(\omega)$	1.27
Ref. [38]	Natural atoms	$\chi_{02}(\omega)$	0.04
Ref. [55]	Natural atoms	$\chi_{02}(\omega)$	0.02

In contrast, the EIT regime does not overlap with the area $\gamma_R \geqslant \frac{1}{2}$. In this area, only ATS can be realized when $\Omega_R > \Omega_M$. We also take three points B_1–B_3 as examples and plot the corresponding $\chi_R''(\delta_R)$ and $\mathrm{Im}[R_\pm(\delta_R)]$ in Figs. 5(d)–5(f), respectively. In Fig. 4, B_1 lies below both curves Ω_W and Ω_M. Thus, in Fig. 5(d), two Lorentzians $\mathrm{Im}[R_\pm(\delta_R)]$ are located at $\delta_R = 0$ with different signs, and $\chi_R''(\delta_R)$ do not exhibit a dip, just as the case in Fig. 5(a). B_2 lies above the curve Ω_W and below the curve Ω_M. Thus, in Fig. 5(e), $\mathrm{Im}[R_\pm(\delta_R)]$ are two positive peaks, but the gap between them is not large enough to make a dip appear in $\chi_R''(\delta_R)$. In contrast, B_3 lies above both curves Ω_W and Ω_M. Thus, in Fig. 5(f), the gap between the two positive peaks $\mathrm{Im}[R_\pm(\delta_R)]$ is large enough to make a dip appear in $\chi_R''(\delta_R)$, similar to the case in Fig. 5(c).

On the basis of the above discussions, now we start to analyze several EIT or ATS experiments in SQCs and natural atoms. In Table I, we summarize the experimental parameters in Refs. [38,49,50,53,55]. We can find that for the experiments in natural atoms, the parameter γ_R is much smaller than $\frac{1}{2}$. As shown in Fig. 3, $\Omega_M(\gamma_R)$ goes down when γ_R decreases. Thus, in these systems, a dip in the susceptibility spectrum can be observed even when a weak driving field is applied, i.e., when $\Omega_R < 1$. Both EIT and ATS can be realized in these systems. In addition, a transition from EIT to ATS has been demonstrated in Ref. [55] by increasing the Rabi frequency of the driving field, similar to the transition from the point A_2 to A_3 in Fig. 4. However, for the experiments in SQCs, the parameter γ_R is larger than $\frac{1}{2}$. Thus, ATS can be realized in these systems but EIT can not. Due to the difference in γ_R, the threshold Ω_M for these experiments in SQCs is much larger than that in natural atoms. Thus, for these experiments in SQCs, the dip in the susceptibility spectrum can only be observed when a driving field much stronger than the damping rates is applied.

From the above discussions, we find that γ_R is an important parameter which makes SQCs and natural atoms differ largely in EIT and ATS experiments. In natural atoms, many energy levels can be used, from which three appropriate energy levels with a γ_R much smaller than the threshold $\frac{1}{2}$ can be found. However, in SQCs usually only the lowest three energy levels are used and γ_R for these three levels are around 1. This difference in γ_R makes it more difficult to realize EIT in SQCs than in natural atoms.

D. Effects of the driving-field detuning Δ and the damping rates γ_{12} and γ_{21}

We now discuss the effects of the driving-field detuning Δ and the damping rates γ_{12} and γ_{21} on the linear response. In this study, we only consider the case when the driving-field detuning Δ and the Rabi frequency $|\Omega_D|$ satisfy the

condition $\Delta \leqslant |\Omega_D| \ll \omega_i$ $(i = 1, 2, 3)$. In addition, the condition $\gamma_{12}, \gamma_{21} \ll |\Omega_D|$ is fulfilled because the coupling between the three-level SFQC and its environment is weak. In this case, the driving-field detuning Δ and the damping rates γ_{12} and γ_{21} only slightly affect the magnetic susceptibilities $\chi_{01}(\omega)$ and $\chi_{02}(\omega)$. Thus, we can approximately use the conditions for realizing EIT and ATS in Eqs. (66)–(69) even when the driving-field detuning Δ is nonzero and the damping rates γ_{12} and γ_{21} are taken into account. However, it is necessary to mention the special effect of the damping rates γ_{12} and γ_{21} on the magnetic susceptibilities $\chi_{01}(\omega)$ and $\chi_{02}(\omega)$. That is, the damping rates γ_{12} and γ_{21} can lead to different heights of the two peaks in the absorption spectrum for ATS. For example, when the conditions in Eq. (67) for realizing ATS in the $|0\rangle \leftrightarrow |1\rangle$ frequency range are fulfilled, and the driving-field detuning Δ is zero, we find that the damping rates γ_{12} and γ_{21} can make the complex roots $\delta_\pm$ have different imaginary parts, i.e., $\mathrm{Re}(\delta_+) = -\mathrm{Re}[\delta_-] \neq 0$ and $\mathrm{Im}(\delta_+) \neq \mathrm{Im}(\delta_-)$. In this case, $\mathrm{Im}[R_+^{(01)}(\delta_1)]$ and $\mathrm{Im}[R_-^{(01)}(\delta_1)]$ are two positive peaks with different heights, resulting in two different heights for the two peaks in the absorption spectrum for ATS. Similar results for ATS in the $|0\rangle \leftrightarrow |2\rangle$ frequency range can also be found.

In Fig. 6, we plot the imaginary parts of the susceptibility $\chi_{01}(\omega_P)$ and the two resonances $R_\pm^{(01)}(\omega_P - \omega_1)$. The parameters in Fig. 6 are appropriately chosen to guarantee that the conditions in Eq. (67) for realizing ATS in the $|0\rangle \leftrightarrow |1\rangle$ frequency range are fulfilled. We find that the nonzero driving-field detuning Δ makes the two absorption peaks have different heights and asymmetric positions (see the black dotted curve in Fig. 6). In addition, we find that two absorption peaks have different heights (see the red solid curve in Fig. 6) when the three-level SFQC is resonantly driven, i.e., $\Delta = 0$, which is in accordance with the above discussions.

Because the transmission coefficient t in Ref. [50] and the magnetic susceptibility $\chi_{01}(\omega)$ in Eq. (60) satisfy the relation $\chi_{01}(\omega) \propto i(1 - t)$, we speculate that this effect of the damping

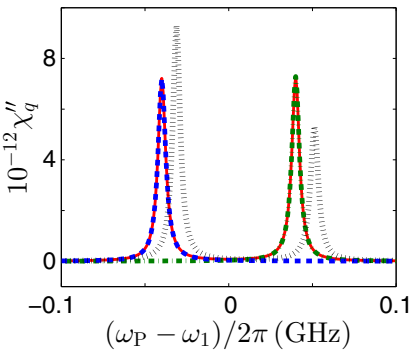

FIG. 6. (Color online) The imaginary parts of $\chi_q(\omega_P)$ (red solid curve), $R_+^{(01)}(\omega_P - \omega_1)$ (blue dashed curve), and $R_-^{(01)}(\omega_P - \omega_1)$ (green dashed-dotted curve) as functions of the detuning of the probe field $\omega_P - \omega_1$ are plotted for $T = 25$ mK and $\Delta = 0$. The imaginary part of $\chi_q(\omega_P)$ is also plotted for $T = 25$ mK, $\Delta/2\pi = 20$ MHz (black dotted curve). Here, we assume that $f = 0.5$, and $|\Omega_D|/2\pi = 40$ MHz. The other parameters of the three-level SFQC are provided in Appendix C.

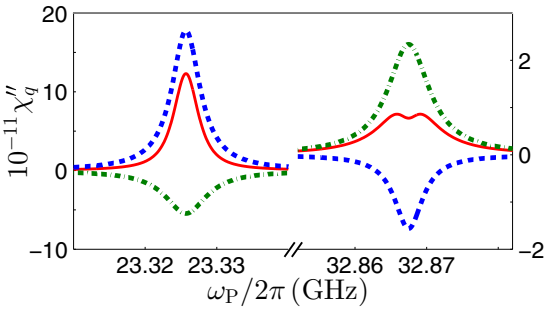

FIG. 7. (Color online) The imaginary part of $\chi_q(\omega_P)$ (red solid curve) is shown as a function of the probe field frequency $\omega_P/2\pi$. In the left part, the imaginary parts of $R_+^{(01)}(\omega_P - \omega_1)$ (blue dashed curve) and $R_-^{(01)}(\omega_P - \omega_1)$ (green dashed-dotted curve) are shown as functions of the probe field frequency $\omega_P/2\pi$. In the right part, the imaginary parts of $R_+^{(02)}(\omega_P - \omega')$ (blue dashed curve) and $R_-^{(02)}(\omega_P - \omega')$ (green dashed-dotted curve) are shown as functions of the probe field frequency $\omega_P/2\pi$. All curves are plotted with $T = 25$ mK and $\Delta = 0$. Here, we assume that $f = 0.525$, and $|\Omega_D|/2\pi = 1.4$ MHz. The other parameters of the three-level SFQC are provided in Appendix C. Note that the left (right) vertical axis is for the left (right) part of the figure.

rates γ_{12} and γ_{21} is a possible reason for the asymmetric transmission spectrum in the ATS experiment [50,51].

E. EIT and ATS in the $|0\rangle \leftrightarrow |1\rangle$ and $|0\rangle \leftrightarrow |2\rangle$ frequency ranges

Now, we study the simultaneous realization of EIT or ATS in both the $|0\rangle \leftrightarrow |1\rangle$ and $|0\rangle \leftrightarrow |2\rangle$ frequency ranges. According to the conditions for realizing EIT (ATS) in Eqs. (66)–(69), EIT can not be realized simultaneously in both the $|0\rangle \leftrightarrow |1\rangle$ and $|0\rangle \leftrightarrow |2\rangle$ frequency ranges because the damping rates γ_{11} and γ_{22} can not satisfy both the conditions $\gamma_{11} > 2\gamma_{22}$ and $\gamma_{22} > 2\gamma_{11}$ in Eqs. (66) and (68). In Fig. 7, the imaginary part of the susceptibility $\chi_q(\omega_P)$ is plotted. The imaginary parts of the two resonances $R_\pm^{(01)}(\omega_P - \omega_1)$ $[R_\pm^{(02)}(\omega_P - \omega')]$, corresponding to $\chi_{01}(\omega_P)$ $[\chi_{02}(\omega_P)]$, are also plotted in the left (right) part of Fig. 7 with the same parameters as for $\chi_q(\omega_P)$. In the right part of Fig. 7, the condition for realizing EIT in the $|0\rangle \leftrightarrow |2\rangle$ frequency range is fulfilled, and EIT is realized when ω_P is near resonant to the $|0\rangle \leftrightarrow |2\rangle$ transition. However, EIT does not occur in the $|0\rangle \leftrightarrow |1\rangle$ frequency range (see the left part of Fig. 7). This is in accordance with our conclusion, i.e., EIT can not be realized simultaneously in both the $|0\rangle \leftrightarrow |1\rangle$ and $|0\rangle \leftrightarrow |2\rangle$ frequency ranges.

However, ATS can be realized simultaneously in both the $|0\rangle \leftrightarrow |1\rangle$ and $|0\rangle \leftrightarrow |2\rangle$ frequency ranges, as long as the Rabi frequency $|\Omega_D|$ is larger than Ω_W, $\Omega_M^{(01)}$, and $\Omega_M^{(02)}$. In Fig. 8, the imaginary part of the susceptibility $\chi_q(\omega_P)$ is plotted. The imaginary parts of the two resonances $R_\pm^{(01)}(\omega_P - \omega_1)$ $[R_\pm^{(02)}(\omega_P - \omega')]$, corresponding to $\chi_{01}(\omega_P)$ $[\chi_{02}(\omega_P)]$, are also plotted in the left (right) part of Fig. 8 with the same parameters as for $\chi_q(\omega_P)$. Here, we set a large $|\Omega_D|$ which fulfills both the conditions for realizing ATS in the $|0\rangle \leftrightarrow |1\rangle$ and $|0\rangle \leftrightarrow |2\rangle$ frequency ranges. Thus, ATS can be realized not only in the

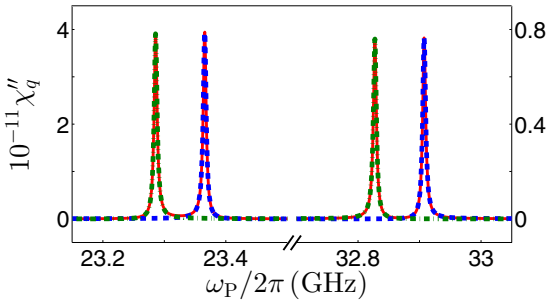

FIG. 8. (Color online) The imaginary part of $\chi_q(\omega_P)$ (red solid curve) is shown as a function of the probe field frequency $\omega_P/2\pi$. In the left part, the imaginary parts of $R_+^{(01)}(\omega_P-\omega_1)$ (blue dashed curve) and $R_-^{(01)}(\omega_P-\omega_1)$ (green dashed-dotted curve) are shown as functions of the probe field frequency $\omega_P/2\pi$. In the right part, the imaginary parts of $R_+^{(02)}(\omega_P-\omega')$ (blue dashed curve) and $R_-^{(02)}(\omega_P-\omega')$ (green dashed-dotted curve) are shown as functions of the probe field frequency $\omega_P/2\pi$. All curves are plotted with $T=25$ mK and $\Delta=0$. Here, we assume that $f=0.525$, and $|\Omega_D|/2\pi=40$ MHz. The other parameters of the three-level SFQC are provided in Appendix C. Note that the left (right) vertical axis is for the left (right) part of the figure.

$|0\rangle \leftrightarrow |1\rangle$ frequency range (see the left part of Fig. 8), but also in the $|0\rangle \leftrightarrow |2\rangle$ frequency range (see the right part of Fig. 8). In this case, there are four absorption peaks and two transparency windows. However, in three-level natural atoms, there are only two absorption peaks and one transparency window for the ATS spectrum.

V. CONCLUSIONS

In conclusion, we have studied the linear response of a three-level SFQC, with a driving field applied to the two upper-energy levels. We include the environmental effect on the three-level SQFC within the Born-Markov approximation. In particular, we study electromagnetically induced transparency (EIT) and Autler-Townes splitting (ATS). We find that when the bias magnetic flux is at the optimal point, the three-level SFQC can respond to the probe field in the frequency range corresponding to the transition between the ground and the first-excited energy levels of the three-level SFQC, like natural atoms with ladder-type transitions. However, when the bias magnetic flux deviates from the optimal point, the three-level SFQC can respond to the probe field in two different frequency ranges, of which one frequency range corresponds to the transition between the ground and the first-excited energy levels of the three-level SFQC, while the other frequency range corresponds to the transition between the ground and the second-excited energy levels of the three-level SFQC. In this case, the three-level SFQC acts like a combination of three-level natural atoms with ladder-type transitions and three-level natural atoms with Λ-type transitions.

We derive the conditions for realizing EIT and ATS in three-level SFQCs. We find that the realization of EIT in a three-level SFQC requires that the damping rates of the three-level SFQC fulfill certain conditions and that the Rabi frequency of the driving field lie in a certain frequency interval defined by the damping rates of the three-level SFQC. Whereas, the realization of ATS in a three-level SFQC only requires that the Rabi frequency of the driving field be large enough. We find that the parameter γ_R, which is defined by the ratio between the damping rates, plays an important role in deciding whether EIT can be realized in three-level systems such as SQCs or natural atoms. We find that $\gamma_R < \frac{1}{2}$ is a necessary condition for realizing EIT. Thus, achieving a system with $\gamma_R < \frac{1}{2}$ should be a prerequisite for EIT experiments in SQCs. Because the values of γ_R in SQCs are usually much larger than those in natural atoms, it is more difficult to demonstrate EIT in SQCs than in natural atoms.

Using the conditions for realizing EIT and ATS, we analyze the linear response of the driven three-level SFQC. When the bias magnetic flux is at the optimal point, EIT (ATS) can be realized in three-level SFQCs like natural atoms with ladder-type transitions [77] if the corresponding condition is fulfilled. When the bias magnetic flux is not at the optimal point, EIT (ATS) can be realized in two different frequency ranges. Each frequency range has its own conditions for realizing EIT (ATS). In addition, EIT can not be realized simultaneously in these two frequency ranges due to the restrictions laid by the conditions for realizing EIT. However, ATS can be realized simultaneously in these two frequency ranges as long as the Rabi frequency of the driving field is large enough.

We also find that the damping rates modified by the driving field can result in two different heights for the two peaks in the ATS absorption spectrum even in the resonant driving. This phenomenon is a possible reason for the asymmetric transmission spectrum in the ATS experiment [50,51].

ACKNOWLEDGMENTS

We thank Dr. A. Smirnov for enlightening discussions. Y.X.L. and J.Q.Y. are supported by the National Basic Research Program of China Grant No. 2014CB921401. Y.X.L. is supported by the NSFC Grants No. 61025022, No. 91321208, and No. 60836001. H.I. is supported by FDCT of Macau under Grant No. 013/2013/A1 and University of Macau under Grant No. MRG022/IH/2013/FST. J.Q.Y. is supported by the NSFC Grant No. 91121015 and the NSAF Grant No. U1330201. E.I. is supported by the European Communitys Seventh Framework Programme (FP7/2007-2013) under Grant No. 270843 (iQIT). F.N. is partially supported by the RIKEN iTHES Project, MURI Center for Dynamic Magneto-Optics, and a Grant-in-Aid for Scientific Research (S).

APPENDIX A: CALCULATIONS OF COMMUTATORS AND ANTICOMMUTATORS

With the assumptions that the coupling between the three-level SFQC and its environment is weak, and that the environmental correlation time τ_c is very small, now we present a concrete method to calculate the commutators and anticommutators in Eqs. (31) and (32).

In the rotating reference frame with the unitary operator shown in Eq. (15), and neglecting the interaction between the three-level SFQC and its environment, the time evolution of the three-level SFQC operators is governed by an effective

Hamiltonian

$$H_{\rm eff} = \hbar\Delta\sigma_{22} + \hbar\Omega_{\rm D}\sigma_{12} + \hbar\Omega_{\rm D}^{*}\sigma_{21} \equiv \varepsilon_1|\tilde{1}\rangle\langle\tilde{1}| + \varepsilon_2|\tilde{2}\rangle\langle\tilde{2}|. \quad \text{(A1)}$$

The eigenvalues of the Hamiltonian in Eq. (A1) $\varepsilon_1 = \hbar(\Delta - \Omega)/2$ and $\varepsilon_2 = \hbar(\Delta + \Omega)/2$ correspond to the eigenstates

$$|\tilde{1}\rangle = \cos(\theta)|1\rangle - \nu^{*}\sin(\theta)|2\rangle, \quad \text{(A2)}$$

$$|\tilde{2}\rangle = \nu\sin(\theta)|1\rangle + \cos(\theta)|2\rangle, \quad \text{(A3)}$$

with the parameter $\nu = \Omega_{\rm D}/|\Omega_{\rm D}|$. The parameter θ, which characterizes the mixing between the states $|1\rangle$ and $|2\rangle$, is given by

$$\tan(\theta) = \sqrt{\frac{\Omega - \Delta}{\Omega + \Delta}}, \quad \text{(A4)}$$

with

$$\Omega = \sqrt{\Delta^2 + 4|\Omega_{\rm D}|^2}. \quad \text{(A5)}$$

Note that the parameter $\theta = 0$ if $|\Omega_{\rm D}| = 0$.

With the effective Hamiltonian in Eq. (A1), the operator $\sigma_{lm}(t')$ at the moment t' evolves to the operator

$$\sigma_{lm}(t) = U_{\rm eff}^{\dagger}(\tau)\sigma_{lm}(t')U_{\rm eff}(\tau), \quad \text{(A6)}$$

with the time interval $\tau = t - t'$. The time-evolution operator $U_{\rm eff}(\tau)$ in Eq. (A6) is

$$U_{\rm eff}(\tau) = |0\rangle\langle 0| + \sum_{l=1}^{2}\exp\left(-i\frac{\varepsilon_l}{\hbar}\tau\right)|\tilde{l}\rangle\langle\tilde{l}|, \quad \text{(A7)}$$

which is given via the effective Hamiltonian in Eq. (A1). Here, the completeness relation $|0\rangle\langle 0| + |\tilde{1}\rangle\langle\tilde{1}| + |\tilde{2}\rangle\langle\tilde{2}| = 1$ has been used in the derivation of Eq. (A7) and the states $|\tilde{l}\rangle$ $(l = 1, 2)$ are given by Eqs. (A2) and (A3). Therefore, all operators $\sigma_{lm}(t')$ at the moment t' can be given by the operators at the moment t via Eqs. (A6) and (A7). The explicit expressions for $\sigma_{lm}(t')$ are listed as follows:

$$\sigma_{00}(t') = \sigma_{00}(t), \quad \text{(A8)}$$

$$\sigma_{11}(t') = |A(\tau)|^2\sigma_{11}(t) + |B(\tau)|^2\sigma_{22}(t) + iA(\tau)B(\tau)\sigma_{12}(t) - iA^{*}(\tau)B^{*}(\tau)\sigma_{21}(t), \quad \text{(A9)}$$

$$\sigma_{22}(t') = |B(\tau)|^2\sigma_{11}(t) + |A(\tau)|^2\sigma_{22}(t) - iA(\tau)B(\tau)\sigma_{12}(t) + iA^{*}(\tau)B^{*}(\tau)\sigma_{21}(t), \quad \text{(A10)}$$

$$\sigma_{01}(t') = e^{i\frac{\Delta}{2}\tau}A^{*}(\tau)\sigma_{01}(t) + ie^{i\frac{\Delta}{2}\tau}B(\tau)\sigma_{02}(t), \quad \text{(A11)}$$

$$\sigma_{02}(t') = ie^{i\frac{\Delta}{2}\tau}B^{*}(\tau)\sigma_{01}(t) + e^{i\frac{\Delta}{2}\tau}A(\tau)\sigma_{02}(t), \quad \text{(A12)}$$

$$\sigma_{12}(t') = iA(\tau)B^{*}(\tau)\sigma_{11}(t) - iA(\tau)B^{*}(\tau)\sigma_{22}(t) + A^{2}(\tau)\sigma_{12}(t) + B^{*2}(\tau)\sigma_{21}(t). \quad \text{(A13)}$$

The expressions for the operators $\sigma_{10}(t')$, $\sigma_{20}(t')$, and $\sigma_{21}(t')$ can be obtained by taking the conjugates of Eqs. (A11)–(A13).

APPENDIX B: EXPRESSIONS FOR Γ_{lm}

The explicit expressions for the complex coefficients Γ_{lm} $(l, m = 1, 2)$ in Eqs. (36) and (37) are given by

$$\Gamma_{11} = |I_{01}|^2A_{11} + |I_{02}|^2A_{12} + |I_{12}|^2A_{13} + (I_{00} - I_{11})I_{00}A_{14} + (I_{00} - I_{11})I_{11}A_{15} + (I_{00} - I_{11})I_{22}A_{16}, \quad \text{(B1)}$$

$$\Gamma_{12} = |I_{01}|^2A_{21} + |I_{12}|^2A_{22} + (I_{00} - I_{11})I_{11}A_{23} + (I_{00} - I_{11})I_{22}A_{24}, \quad \text{(B2)}$$

$$\Gamma_{21} = |I_{02}|^2B_{11} + |I_{12}|^2B_{12} + (I_{00} - I_{22})I_{11}B_{13} + (I_{00} - I_{22})I_{22}B_{14}, \quad \text{(B3)}$$

$$\Gamma_{22} = |I_{01}|^2B_{21} + |I_{02}|^2B_{22} + |I_{12}|^2B_{23} + (I_{00} - I_{22})I_{00}A_{14} + (I_{00} - I_{22})I_{11}A_{16} + (I_{00} - I_{22})I_{22}A_{15}, \quad \text{(B4)}$$

with the parameters

$$A_{11} = 2i\sin^2(\theta)\widetilde{S}(\omega_1^{(+)}) + 2i\cos^2(\theta)\widetilde{S}(\omega_1^{(-)}), \quad \text{(B5)}$$

$$A_{12} = -\frac{\cos^2(\theta)}{2}\Re_{-}(\omega'_{(+)}) - \frac{\sin^2(\theta)}{2}\Re_{-}(\omega'_{(-)}), \quad \text{(B6)}$$

$$A_{13} = \frac{\cos^4(\theta)}{2}\Re_{+}(-\omega_0^{(+)}) + \frac{\sin^4(\theta)}{2}\Re_{+}(-\omega_0^{(-)}) + \frac{\sin^2(2\theta)}{4}\Re_{+}(-\omega_0), \quad \text{(B7)}$$

$$A_{14} = -\frac{1}{2}\Re_{-}(0), \quad \text{(B8)}$$

$$A_{15} = -\frac{\sin^2(2\theta)}{8}\Re_{+}(\Omega) - \frac{\sin^2(2\theta)}{8}\Re_{+}(-\Omega) - \frac{1 + \cos^2(2\theta)}{4}\Re_{+}(0), \quad \text{(B9)}$$

$$A_{16} = \frac{\sin^2(2\theta)}{8}\Re_{+}(\Omega) + \frac{\sin^2(2\theta)}{8}\Re_{+}(-\Omega) - \frac{\sin^2(2\theta)}{4}\Re_{+}(0), \quad \text{(B10)}$$

$$A_{21} = \frac{\nu\sin(2\theta)}{4}\Re_{+}(\omega_1^{(+)}) - \frac{\nu\sin(2\theta)}{4}\Re_{+}(\omega_1^{(-)}), \quad \text{(B11)}$$

$$A_{22} = -\frac{\nu\sin(2\theta)\cos^2(\theta)}{4}\Re_{+}(-\omega_0^{(+)}) + \frac{\nu\sin(2\theta)\sin^2(\theta)}{4}\Re_{+}(-\omega_0^{(-)}) + \frac{\nu\sin(2\theta)\cos(2\theta)}{4}\Re_{+}(-\omega_0), \quad \text{(B12)}$$

$$A_{23} = -\frac{\nu \sin(2\theta)\cos^2(\theta)}{4}\Re_+(\Omega) + \frac{\nu \sin(2\theta)\sin^2(\theta)}{4}\Re_+(-\Omega) + \frac{\nu \sin(2\theta)\cos(2\theta)}{4}\Re_+(0), \quad \text{(B13)}$$

$$A_{24} = \frac{\nu \sin(2\theta)\cos^2(\theta)}{4}\Re_+(\Omega) - \frac{\nu \sin(2\theta)\sin^2(\theta)}{4}\Re_+(-\Omega) - \frac{\nu \sin(2\theta)\cos(2\theta)}{4}\Re_+(0), \quad \text{(B14)}$$

$$B_{11} = \frac{\nu^* \sin(2\theta)}{4}\Re_+(\omega'_{(+)}) - \frac{\nu^* \sin(2\theta)}{4}\Re_+(\omega'_{(-)}), \quad \text{(B15)}$$

$$B_{12} = \frac{\nu^* \sin(2\theta)\cos^2(\theta)}{4}\Re_+(\omega_0^{(+)}) - \frac{\nu^* \sin(2\theta)\sin^2(\theta)}{4}\Re_+(\omega_0^{(-)}) - \frac{\nu^* \sin(2\theta)\cos(2\theta)}{4}\Re_+(\omega_0), \quad \text{(B16)}$$

$$B_{13} = \frac{\nu^* \sin(2\theta)\sin^2(\theta)}{4}\Re_+(\Omega) - \frac{\nu^* \sin(2\theta)\cos^2(\theta)}{4}\Re_+(-\Omega) + \frac{\nu^* \sin(2\theta)\cos(2\theta)}{4}\Re_+(0), \quad \text{(B17)}$$

$$B_{14} = -\frac{\nu^* \sin(2\theta)\sin^2(\theta)}{4}\Re_+(\Omega) + \frac{\nu^* \sin(2\theta)\cos^2(\theta)}{4}\Re_+(-\Omega) - \frac{\nu^* \sin(2\theta)\cos(2\theta)}{4}\Re_+(0), \quad \text{(B18)}$$

$$B_{21} = -\frac{\sin^2(\theta)}{2}\Re_-(\omega_1^{(+)}) - \frac{\cos^2(\theta)}{2}\Re_-(\omega_1^{(-)}), \quad \text{(B19)}$$

$$B_{22} = 2i\cos^2(\theta)\widetilde{S}(\omega'_{(+)}) + 2i\sin^2(\theta)\widetilde{S}(\omega'_{(-)}), \quad \text{(B20)}$$

$$B_{23} = \frac{\cos^4(\theta)}{2}\Re_+(\omega_0^{(+)}) + \frac{\sin^4(\theta)}{2}\Re_+(\omega_0^{(-)}) + \frac{\sin^2(2\theta)}{4}\Re_+(\omega_0). \quad \text{(B21)}$$

Here, the function $\Re_\pm(\omega)$ is defined as

$$\Re_\pm(\omega) = \chi(\omega) \pm 2i\widetilde{S}(\omega). \quad \text{(B22)}$$

And, $\omega_0^{(\pm)}$, $\omega_1^{(\pm)}$, and $\omega'_{(\pm)}$ are given by

$$\omega_0^{(\pm)} = \omega_0 \pm \Omega, \quad \omega_1^{(\pm)} = \omega_1 + \frac{\Delta \pm \Omega}{2},$$

$$\omega'_{(\pm)} = \omega' + \frac{\Delta \pm \Omega}{2}.$$

APPENDIX C: PARAMETERS FOR NUMERICAL CALCULATIONS

Here, we give the parameters of the three-level SFQC used in Figs. 3 and 6–8. Same as in Fig. 2, the ratio between the Josephson energy E_J and the charging energy E_c is chosen as $E_J = 48\,E_c$, and the ratio α between the larger Josephson junction and the smaller one is $\alpha = 0.7$. We set an experimentally accessible Josephson energy $E_J/\hbar = 2\pi \times 144$ GHz. In this case, when the reduced magnetic flux f is at the optimal point, i.e., $f = 0.5$, we can obtain the transition frequencies via Fig. 2(a) as $\omega_1 \approx 0.0257\,E_J/\hbar \approx 2\pi \times 3.69$ GHz, and $\omega_3 \approx 0.1319\,E_J/\hbar \approx 2\pi \times 18.99$ GHz. We can also obtain the matrix elements of the loop current operator $\hat{I}$ via Figs. 2(b) and 2(c) as $|I_{01}| = 0.5617\,I_0$, $|I_{02}| = 0$, $|I_{12}| = 0.2916\,I_0$, and $I_{00} = I_{11} = I_{22} = 0$.

When $f = 0.525$, the corresponding transition frequencies are $\omega_1 \approx 0.162\,E_J/\hbar \approx 2\pi \times 23.33$ GHz and $\omega_3 \approx 0.0663\,E_J/\hbar \approx 2\pi \times 9.54$ GHz, respectively. The corresponding loop current matrix elements are $|I_{01}| = 0.1353\,I_0$, $|I_{02}| = 0.0596\,I_0$, $|I_{12}| = 0.4495\,I_0$, $I_{00} = 0.5883\,I_0$, $I_{11} = -0.1768\,I_0$, and $I_{22} = -0.0467\,I_0$. Here, we note again $I_0 = 2\pi E_J/\Phi_0$.

We assume the cutoff frequency in Eq. (52) as $\omega_c = 100\,\omega_s$, with ω_s corresponding to the transition frequency $\omega_3 = (E_2 - E_0)/\hbar$ when $f = 0.5$. We set a dimensionless constant $\beta = \eta I_s^2/2\pi$, with $I_s \equiv |I_{01}|$ when $f = 0.5$. In this way, the spectral function $\chi''(\omega)$ in Eq. (52) can be expressed as

$$\chi''(\omega) = \frac{\beta}{I_s^2}\,\omega \exp\left(-\frac{|\omega|}{100\omega_s}\right). \quad \text{(C1)}$$

In Figs. 3 and 6–8, we assume $\beta = 10^{-4}$.

[1] Y. Makhlin, G. Schön, and A. Shnirman, Rev. Mod. Phys. **73**, 357 (2001).

[2] G. Wendin and V. S. Shumeiko, in *Handbook of Theoretical and Computational Nanotechnology*, edited by M. Rieth and W. Schommers (American Scientific Publishers, Karlsruhe, Germany, 2006), Chap. 12; arXiv:cond-mat/0508729.

[3] J. Q. You and F. Nori, Phys. Today **58**(11), 42 (2005).

[4] J. Clarke and F. K. Wilhelm, Nature (London) **453**, 1031 (2008).

[5] J. Q. You and F. Nori, Nature (London) **474**, 589 (2011).

[6] I. Buluta, S. Ashhab, and F. Nori, Rep. Prog. Phys. **74**, 104401 (2011).

[7] Z.-L. Xiang, S. Ashhab, J. Q. You, and F. Nori, Rev. Mod. Phys. **85**, 623 (2013).

[8] X. Wen and Y. Yu, Phys. Rev. B **79**, 094529 (2009); L. Du, M. Wang, and Y. Yu, *ibid.* **82**, 045128 (2010); L. Du and Y. Yu, *ibid.* **82**, 144524 (2010); S. Xu, Y. Yu, and G. Z. Sun, *ibid.* **82**, 144526 (2010).

[9] S. N. Shevchenko, S. Ashhab, and F. Nori, Phys. Rep. **492**, 1 (2010); Phys. Rev. B **85**, 094502 (2012).

[10] A. Ferrón, D. Domínguez, and M. J. Sánchez, Phys. Rev. Lett. **109**, 237005 (2012).

[11] W. D. Oliver, Y. Yu, J. C. Lee, K. K. Berggren, L. S. Levitov, and T. P. Orlando, Science **310**, 1653 (2005); D. M. Berns, W. D. Oliver, S. O. Valenzuela, A. V. Shytov, K. K. Berggren, L. S. Levitov, and T. P. Orlando, Phys. Rev. Lett. **97**, 150502 (2006); D. M. Berns, M. S. Rudner, S. O. Valenzuela, K. K. Berggren, W. D. Oliver, L. S. Levitov, and T. P. Orlando, Nature (London) **455**, 51 (2008).

[12] M. Sillanpää, T. Lehtinen, A. Paila, Y. Makhlin, and P. Hakonen, Phys. Rev. Lett. **96**, 187002 (2006).

[13] C. M. Wilson, T. Duty, F. Persson, M. Sandberg, G. Johansson, and P. Delsing, Phys. Rev. Lett. **98**, 257003 (2007); C. M. Wilson, G. Johansson, T. Duty, F. Persson, M. Sandberg, and P. Delsing, Phys. Rev. B **81**, 024520 (2010).

[14] A. Izmalkov, S. H. W. van der Ploeg, S. N. Shevchenko, M. Grajcar, E. Il'ichev, U. Hübner, A. N. Omelyanchouk, and H.-G. Meyer, Phys. Rev. Lett. **101**, 017003 (2008).

[15] M. D. LaHaye, J. Suh, P. M. Echternach, K. C. Schwab, and M. L. Roukes, Nature (London) **459**, 960 (2009).

[16] G. Z. Sun, X. D. Wen, B. Mao, J. Chen, Y. Yu, P. H. Wu, and S. Y. Han, Nat. Commun. **1**, 1 (2010); G. Z. Sun, X. D. Wen, B. Mao, Y. Yu, J. Chen, W. W. Xu, L. Kang, P. H. Wu, and S. Y. Han, Phys. Rev. B **83**, 180507(R) (2011).

[17] J. Q. You, J. S. Tsai, and F. Nori, Phys. Rev. B **68**, 024510 (2003); J. Q. You and F. Nori, *ibid.* **68**, 064509 (2003).

[18] Y. X. Liu, L. F. Wei, and F. Nori, Europhys. Lett. **67**, 941 (2004); Phys. Rev. A **71**, 063820 (2005); **72**, 033818 (2005).

[19] A. Blais, R.-S. Huang, A. Wallraff, S. M. Girvin, and R. J. Schoelkopf, Phys. Rev. A **69**, 062320 (2004).

[20] A. Wallraff, D. I. Schuster, A. Blais, L. Frunzio, R.-S. Huang, J. Majer, S. Kumar, S. M. Girvin, and R. J. Schoelkopf, Nature (London) **431**, 162 (2004).

[21] R. J. Schoelkopf and S. M. Girvin, Nature (London) **451**, 664 (2008).

[22] T. P. Orlando, J. E. Mooij, L. Tian, C. H. van der Wal, L. S. Levitov, S. Lloyd, and J. J. Mazo, Phys. Rev. B **60**, 15398 (1999).

[23] J. Hauss, A. Fedorov, C. Hutter, A. Shnirman, and G. Schön, Phys. Rev. Lett. **100**, 037003 (2008); J. Hauss, A. Fedorov, S. André, V. Brosco, C. Hutter, R. Kothari, S. Yeshwant, A. Shnirman, and G. Schön, New J. Phys. **10**, 095018 (2008).

[24] M. Grajcar, S. H. W. van der Ploeg, A. Izmalkov, E. Il'ichev, H.-G. Meyer, A. Fedorov, A. Shnirman, and G. Schön, Nat. Phys. **4**, 612 (2008).

[25] F. Nori, Nat. Phys. **4**, 589 (2008).

[26] S. Ashhab, J. R. Johansson, A. M. Zagoskin, and F. Nori, New J. Phys. **11**, 023030 (2009).

[27] Y. X. Liu, J. Q. You, L. F. Wei, C. P. Sun, and F. Nori, Phys. Rev. Lett. **95**, 087001 (2005).

[28] F. Deppe, M. Mariantoni, E. P. Menzel, A. Marx, S. Saito, K. Kakuyanagi, H. Tanaka, T. Meno, K. Semba, H. Takayanagi, E. Solano, and R. Gross, Nat. Phys. **4**, 686 (2008).

[29] Z. Zhou, Shih-I Chu, and S. Han, Phys. Rev. B **66**, 054527 (2002).

[30] M. H. S. Amin, A. Yu. Smirnov, and A. Maassen van den Brink, Phys. Rev. B **67**, 100508(R) (2003).

[31] Z. Kis and E. Paspalakis, Phys. Rev. B **69**, 024510 (2004).

[32] C.-P. Yang, Shih-I Chu, and S. Han, Phys. Rev. Lett. **92**, 117902 (2004).

[33] S. O. Valenzuela, W. D. Oliver, D. M. Berns, K. K. Berggren, L. S. Levitov, and T. P. Orlando, Science **314**, 1589 (2006).

[34] J. Q. You, Y. X. Liu, and F. Nori, Phys. Rev. Lett. **100**, 047001 (2008).

[35] J. Q. You, Y. X. Liu, C. P. Sun, and F. Nori, Phys. Rev. B **75**, 104516 (2007).

[36] O. Astafiev, K. Inomata, A. O. Niskanen, T. Yamamoto, Yu. A. Pashkin, Y. Nakamura, and J. S. Tsai, Nature (London) **449**, 588 (2007).

[37] S. E. Harris, J. E. Field, and A. Imamoglu, Phys. Rev. Lett. **64**, 1107 (1990).

[38] K.-J. Boller, A. Imamoglu, and S. E. Harris, Phys. Rev. Lett. **66**, 2593 (1991).

[39] S. E. Harris, Phys. Today **50**(7), 36 (1997).

[40] J. P. Marangos, J. Mod. Opt. **45**, 471 (1998).

[41] M. Fleischhauer, A. Imamoglu, and J. P. Marangos, Rev. Mod. Phys. **77**, 633 (2005).

[42] S. H. Autler and C. H. Townes, Phys. Rev. **100**, 703 (1955).

[43] U. Fano, Phys. Rev. **124**, 1866 (1961).

[44] M. D. Lukin, Rev. Mod. Phys. **75**, 457 (2003).

[45] K. V. R. M. Murali, Z. Dutton, W. D. Oliver, D. S. Crankshaw, and T. P. Orlando, Phys. Rev. Lett. **93**, 087003 (2004).

[46] Z. Dutton, K. V. R. M. Murali, W. D. Oliver, and T. P. Orlando, Phys. Rev. B **73**, 104516 (2006).

[47] H. Ian, Y. X. Liu, and F. Nori, Phys. Rev. A **81**, 063823 (2010).

[48] M. Baur, S. Filipp, R. Bianchetti, J. M. Fink, M. Göppl, L. Steffen, P. J. Leek, A. Blais, and A. Wallraff, Phys. Rev. Lett. **102**, 243602 (2009).

[49] M. A. Sillanpää, J. Li, K. Cicak, F. Altomare, J. I. Park, R. W. Simmonds, G. S. Paraoanu, and P. J. Hakonen, Phys. Rev. Lett. **103**, 193601 (2009); J. Li, G. S. Paraoanu, K. Cicak, F. Altomare, J. I. Park, R. W. Simmonds, M. A. Sillanpää, and P. J. Hakonen, Phys. Rev. B **84**, 104527 (2011); Sci. Rep. **2**, 645 (2012).

[50] A. A. Abdumalikov, Jr., O. Astafiev, A. M. Zagoskin, Yu. A. Pashkin, Y. Nakamura, and J. S. Tsai, Phys. Rev. Lett. **104**, 193601 (2010).

[51] P. M. Anisimov, J. P. Dowling, and B. C. Sanders, Phys. Rev. Lett. **107**, 163604 (2011).

[52] I.-C. Hoi, C. M. Wilson, G. Johansson, J. Lindkvist, B. Peropadre, T. Palomaki, and P. Delsing, New J. Phys. **15**, 025011 (2013).

[53] S. Novikov, J. E. Robinson, Z. K. Keane, B. Suri, F. C. Wellstood, and B. S. Palmer, Phys. Rev. B **88**, 060503(R) (2013).

[54] W. R. Kelly, Z. Dutton, J. Schlafer, B. Mookerji, T. A. Ohki, J. S. Kline, and D. P. Pappas, Phys. Rev. Lett. **104**, 163601 (2010).

[55] L. Giner, L. Veissier, B. Sparkes, A. S. Sheremet, A. Nicolas, O. S. Mishina, M. Scherman, S. Burks, I. Shomroni, D. V. Kupriyanov, P. K. Lam, E. Giacobino, and J. Laurat, Phys. Rev. A **87**, 013823 (2013).

[56] B. Peng, S. K. Ozdemir, W. Chen, F. Nori, and L. Yang, arXiv:1404.5941.

[57] D. V. Averin, Physica C (Amsterdam) **352**, 120 (2001).

[58] A. N. Korotkov and D. V. Averin, Phys. Rev. B **64**, 165310 (2001).

[59] A. Maassen van den Brink, Europhys. Lett. **58**, 562 (2002).
[60] S. Pilgram and M. Büttiker, Phys. Rev. Lett. **89**, 200401 (2002).
[61] Ya. S. Greenberg, A. Izmalkov, M. Grajcar, E. Il'ichev, W. Krech, and H.-G. Meyer, Phys. Rev. B **66**, 224511 (2002).
[62] A. A. Clerk, S. M. Girvin, and A. D. Stone, Phys. Rev. B **67**, 165324 (2003).
[63] E. Il'ichev, Th. Wagner, L. Fritzsch, J. Kunert, V. Schultze, T. May, H. E. Hoenig, H.-G. Meyer, M. Grajcar, D. Born, W. Krech, M. V. Fistul, and A. M. Zagoskin, Appl. Phys. Lett. **80**, 4184 (2002).
[64] M. Grajcar, A. Izmalkov, E. Il'ichev, Th. Wagner, N. Oukhanski, U. Hübner, T. May, I. Zhilyaev, H. E. Hoenig, Ya. S. Greenberg, V. I. Shnyrkov, D. Born, W. Krech, H.-G. Meyer, A. Maassen van den Brink, and M. H. S. Amin, Phys. Rev. B **69**, 060501(R) (2004).
[65] A. Izmalkov, M. Grajcar, E. Il'ichev, Th. Wagner, H.-G. Meyer, A. Yu. Smirnov, M. H. S. Amin, A. Maassen van den Brink, and A. M. Zagoskin, Phys. Rev. Lett. **93**, 037003 (2004).
[66] V. I. Shnyrkov, Th. Wagner, D. Born, S. N. Shevchenko, W. Krech, A. N. Omelyanchouk, E. Il'ichev, and H.-G. Meyer, Phys. Rev. B **73**, 024506 (2006).
[67] G. F. Efremov and A. Yu. Smirnov, Zh. Eksp. Teor. Fiz. **80**, 1071 (1981) [Sov. Phys. JETP **53**, 547 (1981)].
[68] A. Yu. Smirnov, Phys. Rev. B **60**, 3040 (1999).
[69] A. Yu. Smirnov, Phys. Rev. B **67**, 155104 (2003).
[70] A. Yu. Smirnov, Phys. Rev. B **68**, 134514 (2003).
[71] Y. X. Liu, C.-X. Yang, H.-C. Sun, and X.-B. Wang, New J. Phys. **16**, 015031 (2014).
[72] A. O. Caldeira and A. J. Leggett, Phys. Rev. Lett. **46**, 211 (1981).
[73] A. J. Leggett, S. Chakravarty, A. T. Dorsey, M. P. Fisher, A. Garg, and W. Zwerger, Rev. Mod. Phys. **59**, 1 (1987).
[74] H.-P. Breuer and F. Petruccione, *The Theory of Open Quantum Systems* (Oxford University Press, Oxford, 2002).
[75] P. Anisimov and O. Kocharovskaya, J. Mod. Opt. **55**, 3159 (2008).
[76] T. Y. Abi-Salloum, Phys. Rev. A **81**, 053836 (2010).
[77] J. J. Clarke, W. A. van Wijngaarden, and H. Chen, Phys. Rev. A **64**, 023818 (2001).